

# Method of Relaxed Streamlined-Upwinding for Hyperbolic Conservation Laws

Ameya D. Jagtap

*Tata Institute of Fundamental Research - Centre for Applicable Mathematics (TIFR-CAM), Bangalore-560065, India.*

---

## Abstract

In this work a new finite element based Method of Relaxed Streamlined Upwinding is proposed to solve hyperbolic conservation laws. The formulation of the proposed scheme is based on the relaxation system which replaces hyperbolic conservation laws by semi-linear system with stiff source term also called as relaxation term. The advantage of the semi-linear system is that the nonlinearity in the convection term is pushed to the source term on the right hand side which can be handled with ease. Proposed formulation gives an exact diffusion vectors which are very simple. Moreover, the formulation is easily extendable from scalar to vector conservation laws. Various test cases are solved including Burgers equation (with convex and non-convex flux function), Euler equations and shallow water equations in one and two dimensions which demonstrate the robustness, efficiency and accuracy of the proposed scheme. Both four node quadrilateral element and three node triangular element are used to solve multidimensional problems. Error analysis of the proposed scheme shows the optimal convergence rate. Moreover, spectral stability analysis is done which gives the implicit expression for critical time step.

*Keywords:* Finite Element, Relaxation System, Burgers Equation, Euler Equations, Shallow Water Equations, Spectral Stability Analysis.

---

## 1. Introduction

Many natural processes are governed by hyperbolic conservation laws like high speed flows governed by inviscid Euler equations, shallow water flows like flow in a canal, river flows *etc* are governed by shallow water equations, astrophysical flows or space weather governed by magnetohydrodynamic equations *etc*. These equations describes the transport and propagation of waves (both linear and nonlinear) in space and time. Due to nonlinear nature of convection term such equations admits discontinuous solution which precludes the possibility of finding closed form solution for such equations. Alternatively, numerical methods are used to solve these equations. In the literature of finite volume and finite difference framework upwind methods are extensively used to solve hyperbolic conservation laws. Riemann solvers are one of the popular class of upwind schemes. Apart from Riemann solvers there are other upwind methods available in the literature like flux splitting methods, kinetic schemes and relaxation schemes. Upwind methods are also used in finite element framework where they are the part of much larger group called as stabilized finite element methods which are used to solve hyperbolic conservation laws. There are various stabilized finite element methods available in the literature like Taylor Galerkin method, Streamlined-Upwind Petrov-Galerkin (SUPG) method, Discontinuous Galerkin method, Least-Square Galerkin method *etc*. For more details about these methods see [1, 3, 2, 4, 5]. Among all methods, SUPG method is one of the oldest stabilized scheme derived for convection dominated flows. Due to their desirable properties SUPG scheme is widely used stabilized finite element method for both compressible [51, 52, 53] as well as incompressible flow [47, 48] (along with Pressure Stabilizing Petrov Galerkin PSPG formulation [50]). Different versions of SUPG scheme were derived like, conservative variable and entropy variable based SUPG scheme [54, 55]. Kinetic theory based SUPG method called as Kinetic Streamlined-Upwind Petrov-Galerkin (KSUPG) method is also developed for Burgers equation and Euler equations

---

\*Corresponding author

Email address: ameya.aero@gmail.com, ameya@tifrbng.res.in (Ameya D. Jagtap)

of gas dynamics [8]. KSUPG method overcomes some of the shortcomings of classical SUPG method like finding the unique diffusion vectors and intrinsic time scale, especially, for multidimensional vector conservation laws.

Relaxation schemes introduced by Jin & Xin [9] for hyperbolic conservation laws without source term are an attractive alternative to the other upwinds schemes. In the recent years, the simplicity of this scheme attracted many researchers around the world. Relaxation scheme is based on the relaxation system which replaces nonlinear convection term present in hyperbolic partial differential equation(s) by semilinear system with stiff relaxation term on right hand side. This system is equivalent to original hyperbolic conservation law in the limit of vanishing relaxation parameter. The simple procedure present in Relaxation schemes to handle nonlinear convection term avoids more complex Riemann solvers, kinetic schemes and flux splitting methods. First and second order relaxation schemes were first introduced in [9] while the higher order relaxation schemes are discussed in [11, 12, 13]. The relaxation scheme for a hyperbolic conservation laws with source term are presented in [14, 15, 16]. Natalini [17] interpreted Jin & Xin's relaxation system as a discrete velocity Boltzmann equation with BGK model for the collision term. In [19] Aregba-Driollet and Natalini introduced numerical schemes based on discrete velocity Boltzmann equation which are called as discrete velocity kinetic schemes. Relaxation schemes are also employed in the lattice Boltzmann framework [26, 27]. An alternative relaxation system for one dimensional conservation law proposed by Murthy [10] retain the semilinear structure of original relaxation system but at the same time satisfies the integral constraint which is more consistent than the original relaxation system. For more details about the relaxation schemes refer [9, 18, 17, 19, 20, 22, 23, 24, 25, 30] and the references there in.

Relaxation scheme is also used in finite element framework [28] for one dimensional scalar and vector (elastodynamics) problems. In this paper the relaxation based Streamlined-Upwind scheme, named as Method of Relaxed Streamlined-Upwinding (MRSU) is developed in finite element framework for hyperbolic conservation laws in one and two dimensions. Some of the silent features of proposed formulation are

1. The weak formulation of governing hyperbolic PDEs is started in conservation form which is obtained from relaxation system with an analogous procedure used in Relaxed scheme (instantaneous relaxation).
2. Only test space of convection part of the governing equation is enriched to obtain the required stabilization term.
3. In this analysis, group discretization or group formulation of flux function which are shown to be more accurate is used [41, 42].
4. Proposed scheme can be easily extended from scalar to vector conservation laws.
5. Another advantage of MRSU scheme is, exact stabilization vectors can be obtained for both scalar as well as vector conservation laws. Importantly, no Jacobian matrices are involved in the stabilization terms.
6. Various symmetric relaxation models are proposed for two dimensional system which includes four point along diagonal ( $\mathcal{D}4$ ), nine point ( $\mathcal{A}\mathcal{D}9$ ) and four point along axis ( $\mathcal{A}4$ ) discrete velocity models.
7. Temporal discretization is done by using simple first order forward Euler method.
8. To show the efficacy of the proposed scheme various test cases of scalar and vector hyperbolic conservation laws like Burgers equation, Euler equations and shallow water equations are solved for one and two dimensional problems.
9. Error analysis is done which shows optimal rate of convergence. Furthermore, spectral stability analysis is done which gives the implicit expression for critical time step.

This paper is arranged as follows. After introduction in section 1, section 2 describes the governing hyperbolic conservation laws like Burgers equation, Euler and shallow water equations. Section 3 gives the relaxed formulation for hyperbolic conservation laws which will be useful in developing MRSU scheme. Section 4 explains two and three discrete velocity model for one dimensional equations. Section 5 describe various symmetric relaxation systems for two dimensional problems followed by section 6 where Chapman-Enskog expansion of relaxation system is described which gives conditions for stability of such systems. Section 7 gives the weak formulation of MRSU scheme. Section 8 describes the temporal discretization followed by section 9 which describes about shock capturing parameter. In section 10 spectral stability analysis of the proposed scheme is done which is followed by section 11 where numerical experiments are carried out for various test cases. This paper is concluded in section 12.

## 2. Hyperbolic Conservation Laws

In this paper we shall consider Burgers equation, compressible Euler equations and Shallow water equations in both one and two dimensions. These equations are given as

$$\frac{\partial U}{\partial t} + \frac{\partial G_i(U)}{\partial x_i} = 0 \in \mathbb{R}^D \times \mathbb{R}^+$$

where  $U$  is a solution vector and flux vectors  $G_i(U)$  are functions of  $U$ . In case of Burgers equation both  $U$  and  $G_i$ 's are scalar quantities. In case of Euler equations  $U$  and  $G_i$ 's are given as  $U = [\rho, \rho u_1, \rho u_2, \rho u_3, \rho E]^T$  and  $G_i = [\rho u_i, \delta_{i1}p + \rho u_1 u_i, \delta_{i2}p + \rho u_2 u_i, \delta_{i3}p + \rho u_3 u_i, \rho u_i + \rho u_i E]^T$  where  $\rho, u_1, u_2, u_3, E, p$  are density, velocity components in  $x, y$  and  $z$  directions, total energy and pressure respectively and  $\delta_{ij}$  is a kronecker delta. Total energy is given by

$$E = \frac{p}{\rho(\gamma - 1)} + \frac{1}{2} \|\mathbf{u}\|_{\mathcal{L}_2}^2$$

The eigenvalues of flux Jacobian matrices  $A_i = \frac{\partial G_i}{\partial U}$  are

$$u_i \pm a, u_i, u_i, u_i,$$

where  $a = \sqrt{\gamma p / \rho}$  is acoustic speed.

For shallow water equations  $U$  and  $G_i$ 's are given as  $U = [h, hu_1, hu_2]^T$  and  $G_i = [hu_i, hu_1 u_i + \delta_{i1} 0.5gh^2, hu_2 u_i + \delta_{i2} 0.5gh^2]^T$  where  $h, u_1, u_2, g$  are water height, velocity components in  $x$  and  $y$  directions and gravity respectively. Here eigenvalues of flux Jacobian matrices  $A_i = \frac{\partial G_i}{\partial U}$  are

$$u_i \pm \sqrt{gh}, u_i$$

## 3. Relaxed Formulation for Hyperbolic Conservation Laws

Consider the following hyperbolic conservation law in 1D

$$\frac{\partial U}{\partial t} + \frac{\partial G(U)}{\partial x} = 0 \in \mathbb{R} \times \mathbb{R}^+$$

with initial conditions

$$U(x, 0) = U_0(x)$$

where  $U \in \mathbb{R}^n$  and  $G(U) \in \mathbb{R}^n$ . Jin and Xin [9] proposed the following relaxation system for above equation

$$\begin{aligned} \frac{\partial U}{\partial t} + \frac{\partial W}{\partial x} &= 0 \\ \frac{\partial W_i}{\partial t} + \Lambda^2 \frac{\partial U}{\partial x} &= \frac{1}{\epsilon} (G(U) - W) \end{aligned}$$

with initial conditions

$$U(x, 0) = U_0(x), \quad W(x, 0) = G(U_0(x))$$

where  $W \in \mathbb{R}^m, \Lambda^2 \in \mathbb{R}^{m \times m}$  is a diagonal matrix with non-negative elements and  $\epsilon$  is the relaxation time. The advantage of above relaxation system is convection term is linear. Nonlinearity is moved in the source term shown by right hand side. The relaxation system can be solved using splitting method where the system is split into linear partial differential equations and nonlinear ordinary differential equations [9]. Above set of equations can be written in matrix form as

$$\frac{\partial Q}{\partial t} + A \frac{\partial Q}{\partial x} = H$$

where

$$Q = \begin{Bmatrix} U \\ W \end{Bmatrix}, \quad A = \begin{bmatrix} 0 & 1 \\ \Lambda^2 & 0 \end{bmatrix}, \quad H = \begin{Bmatrix} 0 \\ \frac{1}{\epsilon} (G(U) - W) \end{Bmatrix}$$

Matrix  $A$  can be decomposed as

$$A = R\Lambda R^{-1}$$

where  $R$  is a modal matrix whose columns are the eigenvectors of  $A$  and  $\Lambda$  is a spectral matrix with eigenvalues as diagonal entries. Introducing the Characteristics variable vector  $\mathbf{f} = R^{-1}Q$  above system can be written as

$$\frac{\partial \mathbf{f}}{\partial t} + \Lambda \frac{\partial \mathbf{f}}{\partial x} = R^{-1}H \quad (1)$$

where

$$\mathbf{f} = R^{-1}Q = \begin{Bmatrix} f_1 \\ f_2 \end{Bmatrix} = \begin{Bmatrix} \frac{U}{2} - \frac{W}{2\lambda} \\ \frac{U}{2} + \frac{W}{2\lambda} \end{Bmatrix}$$

From this, variables  $U$  and  $W$  can be recovered as

$$U = f_1 + f_2, \quad W = \lambda(f_2 - f_1)$$

Let

$$\mathbf{F} = \begin{Bmatrix} F_1 \\ F_2 \end{Bmatrix} = \begin{Bmatrix} \frac{U}{2} - \frac{G}{2\lambda} \\ \frac{U}{2} + \frac{G}{2\lambda} \end{Bmatrix} \quad (2)$$

using this equation (1) can be written as

$$\frac{\partial \mathbf{f}}{\partial t} + \Lambda \frac{\partial \mathbf{f}}{\partial x} = -\frac{(\mathbf{f} - \mathbf{F})}{\epsilon} \quad (3)$$

with initial conditions

$$U(x, 0) = U_0(x), \quad \mathbf{f}(0) = \mathbf{F}(U_0(x))$$

For small value of  $\epsilon$  above equation looks similar to the classical Boltzmann equation with BGK model where  $\epsilon$  is performing a role of relaxation time. Here  $\mathbf{f}$  represents the distribution function whereas  $\mathbf{F}$  represents local Maxwellian distribution. In the above equation discrete velocities  $-\lambda$  and  $\lambda$  are involved whereas in a classical Boltzmann equation velocities are continuous. Due to this Natalini [19] interpreted relaxation system (equation (3)) as a discrete velocity Boltzmann equation.

Splitting method can be employed to solve equation (3) which can be written in two steps as

$$\begin{aligned} \frac{\partial \mathbf{f}}{\partial t} + \Lambda \frac{\partial \mathbf{f}}{\partial x} &= 0 & : \text{Convection} \\ \frac{d\mathbf{f}}{dt} &= -\frac{(\mathbf{f} - \mathbf{F})}{\epsilon} & : \text{Relaxation} \end{aligned}$$

The solution of relaxation step is  $\mathbf{f} = (\mathbf{f}(0) - \mathbf{F})e^{-t/\epsilon} + \mathbf{F}$ . Assuming that the relaxation is instantaneous  $\epsilon = 0$  which gives  $\mathbf{f} = \mathbf{F}$ . Thus, we recover following convection equation

$$\frac{\partial \mathbf{F}}{\partial t} + \Lambda \frac{\partial \mathbf{F}}{\partial x} = 0$$

which can be rewritten in conservation form as

$$\frac{\partial \mathbf{F}}{\partial t} + \frac{\partial P\mathbf{F}}{\partial x} = 0 \quad (4)$$

Conservative variables at macroscopic level are recovered by taking moments

$$\frac{\partial P\mathbf{F}}{\partial t} + \frac{\partial P\Lambda\mathbf{F}}{\partial x} = 0$$

where

$$P\mathbf{F} = U, \quad P\Lambda\mathbf{F} = G \quad (5)$$

and  $P = [1, 1, \dots \text{No. of discrete Velocities}]$ . Schemes based on above procedure are called as instantaneous Relaxation schemes or Relaxed schemes.

#### 4. Two and Three Discrete Velocity Model for 1D Hyperbolic Conservation Laws

We shall consider two discrete velocity model for one dimensional hyperbolic conservation laws namely, Two and Three Discrete Velocity Models.

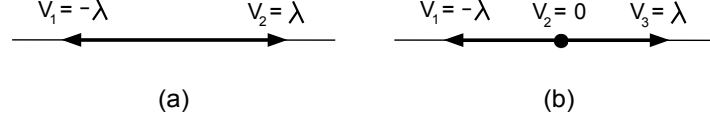


Figure 1: (a) Two discrete velocity and (b) three discrete velocity models

In case of two velocity model two moving particles are present and  $\Lambda$  is given as

$$\Lambda = \begin{bmatrix} -\lambda & 0 \\ 0 & \lambda \end{bmatrix}$$

and the corresponding expression for  $\mathbf{F}$  is given by equation (2) which satisfies the moment relations (equation (5)). In case of three velocity model there is a rest particle along with two moving particle. In this case  $\Lambda$  is given as

$$\Lambda = \begin{bmatrix} -\lambda & 0 & 0 \\ 0 & 0 & 0 \\ 0 & 0 & \lambda \end{bmatrix}$$

Expression for  $\mathbf{F}$  is given by

$$\mathbf{F} = \begin{Bmatrix} F_1 \\ F_2 \\ F_3 \end{Bmatrix} = \begin{Bmatrix} \frac{U}{3} - \frac{G}{2\lambda} \\ \frac{U}{3} \\ \frac{U}{3} + \frac{G}{2\lambda} \end{Bmatrix}$$

Again, this satisfies the moment relations. Detailed derivation of  $\mathbf{F}$  for three velocity model is given in Appendix. Figure 1 (a) and (b) shows two and three discrete velocity models respectively.

#### 5. Symmetric Discrete Velocity Models for Multidimensional Conservation Laws

Asymmetric discrete velocity model for multidimensional relaxation system is discussed in the literature [19]. In this section we shall consider the symmetric relaxation system (involving symmetric discrete velocity models) in two dimension which takes information symmetrically from all directions. In two dimensional problems there are various choices for symmetric relaxation system possible.  $\Lambda$  matrices are constructed using  $N$  diagonal blocks as

$$\Lambda_i = \text{diag}(\lambda_1^{(i)}, \lambda_2^{(i)}, \dots, \lambda_N^{(i)})$$

In order to admit kinetic entropy and satisfy the entropy inequality in the equilibrium limit  $\epsilon \rightarrow 0$  by equation (3), Bochut [21] has characterized the space of Maxwellians. The Maxwellians are written as a linear combination of conserved variables and fluxes as

$$F_i(U) = k_{i0}U + \sum_{j=1}^{\mathcal{D}} k_{ij}G_j(U) \text{ for } i = 1, 2, \dots, N$$

where constants  $k_{ij}$  are chosen in such a way that consistency condition given by equations (5) is satisfied. The  $\Lambda$  matrices are constructed using orthogonal velocity method [9]. Here, diagonal entries  $\lambda_j^{(i)}$ 's are chosen such that they satisfy following two conditions

$$\sum_{j=1}^N \lambda_j^{(i)} = 0, \quad \forall i = 1, 2, \dots, \mathcal{D}$$

$$\sum_{l=1}^N \lambda_l^{(i)} \lambda_l^{(j)} = 0, \quad \text{where } i \neq j \text{ and } \forall i, j = 1, 2, \dots, \mathcal{D}$$

with this the Maxwellian is obtained as

$$F_i(U) = \frac{U}{N} + \sum_{j=1}^{\mathcal{D}} \frac{G_j(U)}{\left(\sum_{l=1}^N |\lambda_l^{(j)}|\right)} \text{sgn}(\lambda_l^{(j)})$$

Now, let's consider different symmetric relaxation system for two dimensional conservation laws. In this case three symmetric relaxation system models are proposed viz., four point along diagonal ( $\mathcal{D}4$ ) with  $N = 4$ , nine point ( $\mathcal{A}\mathcal{D}9$ ) with  $N = 9$  and four point along axis ( $\mathcal{A}4$ ) with  $N = 4$  discrete velocity based relaxation system as shown in figure 2.

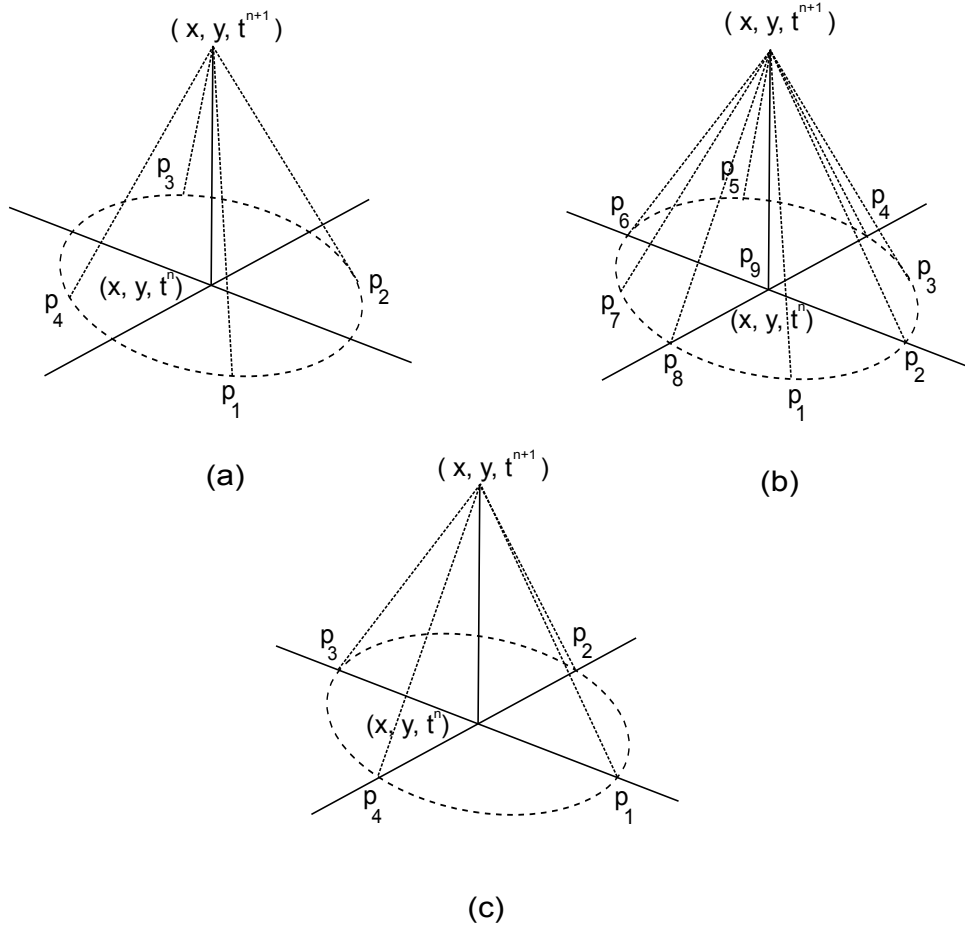


Figure 2: (a) Four point along diagonal ( $\mathcal{D}4$ ), (b) nine point ( $\mathcal{A}\mathcal{D}9$ ) and (c) four point along axis ( $\mathcal{A}4$ ) symmetric relaxation system

$\mathcal{D}4$  symmetric relaxation system uses four characteristics speeds along diagonal from the four quadrant as shown in figure 2 (a) and they are given as

$$\Lambda_1 = \begin{bmatrix} -\lambda_1 & 0 & 0 & 0 \\ 0 & \lambda_1 & 0 & 0 \\ 0 & 0 & \lambda_1 & 0 \\ 0 & 0 & 0 & -\lambda_1 \end{bmatrix}, \quad \Lambda_2 = \begin{bmatrix} -\lambda_2 & 0 & 0 & 0 \\ 0 & -\lambda_2 & 0 & 0 \\ 0 & 0 & \lambda_2 & 0 \\ 0 & 0 & 0 & \lambda_2 \end{bmatrix}$$

The characteristics variable and local Maxwellian distribution function are obtained as

$$\mathbf{f} = \begin{Bmatrix} f_1 \\ f_2 \\ f_3 \\ f_4 \end{Bmatrix} = \begin{Bmatrix} \frac{U}{4} - \frac{W_1(U)}{4\lambda_1} - \frac{W_2(U)}{4\lambda_2} \\ \frac{U}{4} + \frac{W_1(U)}{4\lambda_1} - \frac{W_2(U)}{4\lambda_2} \\ \frac{U}{4} + \frac{W_1(U)}{4\lambda_1} + \frac{W_2(U)}{4\lambda_2} \\ \frac{U}{4} - \frac{W_1(U)}{4\lambda_1} + \frac{W_2(U)}{4\lambda_2} \end{Bmatrix}, \quad \mathbf{F} = \begin{Bmatrix} F_1 \\ F_2 \\ F_3 \\ F_4 \end{Bmatrix} = \begin{Bmatrix} \frac{U}{4} - \frac{G_1(U)}{4\lambda_1} - \frac{G_2(U)}{4\lambda_2} \\ \frac{U}{4} + \frac{G_1(U)}{4\lambda_1} - \frac{G_2(U)}{4\lambda_2} \\ \frac{U}{4} + \frac{G_1(U)}{4\lambda_1} + \frac{G_2(U)}{4\lambda_2} \\ \frac{U}{4} - \frac{G_1(U)}{4\lambda_1} + \frac{G_2(U)}{4\lambda_2} \end{Bmatrix}$$

$\mathcal{A}9$  symmetric relaxation system uses nine characteristics speeds (including rest particle) from the four quadrant as shown in figure 2 (b).

$$\Lambda_1 = \begin{bmatrix} -\lambda_1 & 0 & 0 & 0 & 0 & 0 & 0 & 0 & 0 \\ 0 & 0 & 0 & 0 & 0 & 0 & 0 & 0 & 0 \\ 0 & 0 & \lambda_1 & 0 & 0 & 0 & 0 & 0 & 0 \\ 0 & 0 & 0 & \lambda_1 & 0 & 0 & 0 & 0 & 0 \\ 0 & 0 & 0 & 0 & \lambda_1 & 0 & 0 & 0 & 0 \\ 0 & 0 & 0 & 0 & 0 & 0 & 0 & 0 & 0 \\ 0 & 0 & 0 & 0 & 0 & 0 & -\lambda_1 & 0 & 0 \\ 0 & 0 & 0 & 0 & 0 & 0 & 0 & -\lambda_1 & 0 \\ 0 & 0 & 0 & 0 & 0 & 0 & 0 & 0 & 0 \end{bmatrix},$$

$$\Lambda_2 = \begin{bmatrix} -\lambda_2 & 0 & 0 & 0 & 0 & 0 & 0 & 0 & 0 \\ 0 & -\lambda_2 & 0 & 0 & 0 & 0 & 0 & 0 & 0 \\ 0 & 0 & -\lambda_2 & 0 & 0 & 0 & 0 & 0 & 0 \\ 0 & 0 & 0 & 0 & 0 & 0 & 0 & 0 & 0 \\ 0 & 0 & 0 & 0 & \lambda_2 & 0 & 0 & 0 & 0 \\ 0 & 0 & 0 & 0 & 0 & \lambda_2 & 0 & 0 & 0 \\ 0 & 0 & 0 & 0 & 0 & 0 & \lambda_2 & 0 & 0 \\ 0 & 0 & 0 & 0 & 0 & 0 & 0 & 0 & 0 \\ 0 & 0 & 0 & 0 & 0 & 0 & 0 & 0 & 0 \end{bmatrix}$$

In this case the characteristics variable and local Maxwellian distribution function are obtained as

$$\mathbf{f} = \begin{Bmatrix} f_1 \\ f_2 \\ f_3 \\ f_4 \\ f_5 \\ f_6 \\ f_7 \\ f_8 \\ f_9 \end{Bmatrix} = \begin{Bmatrix} \frac{U}{9} - \frac{W_1(U)}{9\lambda_1} - \frac{W_2(U)}{9\lambda_2} \\ \frac{U}{9} - \frac{W_2(U)}{9\lambda_2} \\ \frac{U}{9} + \frac{W_1(U)}{9\lambda_1} - \frac{W_2(U)}{9\lambda_2} \\ \frac{U}{9} + \frac{W_1(U)}{9\lambda_1} \\ \frac{U}{9} + \frac{W_1(U)}{9\lambda_1} + \frac{W_2(U)}{9\lambda_2} \\ \frac{U}{9} + \frac{W_2(U)}{9\lambda_2} \\ \frac{U}{9} - \frac{W_1(U)}{9\lambda_1} + \frac{W_2(U)}{9\lambda_2} \\ \frac{U}{9} - \frac{W_1(U)}{9\lambda_1} \\ \frac{U}{9} \end{Bmatrix}, \quad \mathbf{F} = \begin{Bmatrix} F_1 \\ F_2 \\ F_3 \\ F_4 \\ F_5 \\ F_6 \\ F_7 \\ F_8 \\ F_9 \end{Bmatrix} = \begin{Bmatrix} \frac{U}{9} - \frac{G_1(U)}{9\lambda_1} - \frac{G_2(U)}{9\lambda_2} \\ \frac{U}{9} - \frac{G_2(U)}{9\lambda_2} \\ \frac{U}{9} + \frac{G_1(U)}{9\lambda_1} - \frac{G_2(U)}{9\lambda_2} \\ \frac{U}{9} + \frac{G_1(U)}{9\lambda_1} \\ \frac{U}{9} + \frac{G_1(U)}{9\lambda_1} + \frac{G_2(U)}{9\lambda_2} \\ \frac{U}{9} + \frac{G_2(U)}{9\lambda_2} \\ \frac{U}{9} - \frac{G_1(U)}{9\lambda_1} + \frac{G_2(U)}{9\lambda_2} \\ \frac{U}{9} - \frac{G_1(U)}{9\lambda_1} \\ \frac{U}{9} \end{Bmatrix}$$

Finally,  $\mathcal{A}4$  symmetric relaxation system uses four characteristics speeds along axis from the four quadrant as shown in figure 2 (c) which are given as

$$\Lambda_1 = \begin{bmatrix} 0 & 0 & 0 & 0 \\ 0 & \lambda_1 & 0 & 0 \\ 0 & 0 & 0 & 0 \\ 0 & 0 & 0 & -\lambda_1 \end{bmatrix}, \quad \Lambda_2 = \begin{bmatrix} -\lambda_2 & 0 & 0 & 0 \\ 0 & 0 & 0 & 0 \\ 0 & 0 & \lambda_2 & 0 \\ 0 & 0 & 0 & 0 \end{bmatrix}$$

In this case characteristics variable and local Maxwellian distribution function are obtained as

$$\mathbf{f} = \begin{pmatrix} f_1 \\ f_2 \\ f_3 \\ f_4 \end{pmatrix} = \begin{pmatrix} \frac{U}{4} - \frac{W_2(U)}{4\lambda_2} \\ \frac{U}{4} + \frac{W_1(U)}{4\lambda_1} \\ \frac{U}{4} + \frac{W_2(U)}{4\lambda_2} \\ \frac{U}{4} - \frac{W_1(U)}{4\lambda_1} \end{pmatrix}, \quad \mathbf{F} = \begin{pmatrix} F_1 \\ F_2 \\ F_3 \\ F_4 \end{pmatrix} = \begin{pmatrix} \frac{U}{4} - \frac{G_2(U)}{4\lambda_2} \\ \frac{U}{4} + \frac{G_1(U)}{4\lambda_1} \\ \frac{U}{4} + \frac{G_2(U)}{4\lambda_2} \\ \frac{U}{4} - \frac{G_1(U)}{4\lambda_1} \end{pmatrix}$$

In all the three models, the macroscopic variables are recovered by taking moments as

$$P\mathbf{F} = U, \quad P\Lambda_i\mathbf{F} = G_i(U)$$

## 6. Chapman-Enskog Type Expansion of Symmetric Relaxation System

Stability condition for 1D scalar hyperbolic conservation law is obtained using Chapman-Enskog type analysis [14] which turn out to be

$$\lambda \geq \sqrt{(g'(u))^2} \geq -\lambda$$

for two discrete velocity model. For three discrete velocity model it becomes

$$\frac{2}{3}\lambda \geq \sqrt{(g'(u))^2} \geq -\frac{2}{3}\lambda$$

For 2D scalar conservation law Chapman-Enskog type analysis can be done to obtain the stability conditions for all the three models. Following the same procedure given in [14] one can write the relaxation system for 2D scalar conservation law as

$$\begin{aligned} \frac{\partial u}{\partial t} + \frac{\partial g_1(u)}{\partial x} + \frac{\partial g_2(u)}{\partial y} &= \epsilon \frac{\partial}{\partial x} \left( \frac{\partial u}{\partial x} [P\Lambda_1^2\mathbf{F}' - (g'_1(u))^2] + \frac{\partial u}{\partial y} [P\Lambda_1\Lambda_2\mathbf{F}' - g'_1(u)g'_2(u)] \right) \\ &+ \epsilon \frac{\partial}{\partial y} \left( \frac{\partial u}{\partial x} [P\Lambda_1\Lambda_2\mathbf{F}' - g'_1(u)g'_2(u)] + \frac{\partial u}{\partial y} [P\Lambda_2^2\mathbf{F}' - (g'_2(u))^2] \right) + O(\epsilon^2) \end{aligned}$$

Table 1 gives expressions for the terms involved in the coefficient of diffusion for various symmetric relaxation models

Symmetric Model	$P\Lambda_1^2\mathbf{F}'$	$P\Lambda_1\Lambda_2\mathbf{F}'$	$P\Lambda_2\Lambda_1\mathbf{F}'$	$P\Lambda_2^2\mathbf{F}'$
$\mathcal{D}4$	$\lambda^2$	0	0	$\lambda^2$
$\mathcal{A}\mathcal{D}9$	$\frac{2}{3}\lambda^2$	0	0	$\frac{2}{3}\lambda^2$
$\mathcal{A}4$	$\frac{1}{2}\lambda^2$	0	0	$\frac{1}{2}\lambda^2$

Table 1: Coefficient of diffusion for symmetric relaxation models.

Thus, to make dissipation positive following conditions must be satisfied

$$\lambda \geq \sqrt{\frac{[(g'_1(u))^2 + (g'_2(u))^2]}{\beta}} \geq -\lambda$$

where  $\beta$  is the coefficient of numerical diffusion ( $\lambda^2$ ).  $\beta = 1, 2/3, 1/2$  for  $\mathcal{D}4, \mathcal{A}\mathcal{D}9, \mathcal{A}4$  models respectively.

For vector conservation laws the stability condition can be obtained following [56, 58, 61]. It can be shown that the solution of the relaxation system approaches exact solution of original hyperbolic partial differential equation as  $\epsilon \rightarrow 0$  if the following sub-characteristics conditions is satisfied

$$\frac{\sigma_1^2}{\Lambda_1^2} + \frac{\sigma_2^2}{\Lambda_2^2} + \dots + \frac{\sigma_n^2}{\Lambda_n^2} \leq 1$$

where  $\sigma_i$ 's are the eigenvalues of Jacobian matrix  $\frac{\partial G}{\partial U}$ . Following values of  $\lambda$  based on the supremum eigenvalue of Jacobian matrices are chosen for Euler and shallow water equations.

For 1D Euler equations

$$\lambda = \max(\sup|u + a|, \sup|u|, \sup|u - a|)$$

and for 1D shallow water equations

$$\lambda = \max(\sup|u + \sqrt{gh}|, \sup|u - \sqrt{gh}|)$$

In case of 2D Euler equations

$$\lambda_1 = \max(\sup|u_1 + a|, \sup|u_1|, \sup|u_1 - a|)$$

$$\lambda_2 = \max(\sup|u_2 + a|, \sup|u_2|, \sup|u_2 - a|)$$

and for 2D shallow water equations

$$\lambda_1 = \max(\sup|u_1 + \sqrt{gh}|, \sup|u_1|, \sup|u - \sqrt{gh}|)$$

$$\lambda_2 = \max(\sup|u_2 + \sqrt{gh}|, \sup|u_2|, \sup|u_2 - \sqrt{gh}|)$$

## 7. Weak MRSU formulation for Hyperbolic Conservation Laws

The standard Galerkin finite element approximation for equilibrium distribution function  $\mathbf{F}$  and the flux function  $\Lambda_j \mathbf{F}$  are

$$\mathbf{F} \approx \mathbf{F}^h = \sum_{\forall i} N_i^h \mathbf{F}_i, \quad \Lambda_j \mathbf{F} \approx (\Lambda_j \mathbf{F})^h = \sum_{\forall i} N_i^h (\Lambda_j \mathbf{F})_i$$

where group formulation is used for flux function. Interpolation function  $N^h \in C^0(\Omega)$  and the computational domain  $\Omega$  is divided into  $Nel$  number of elements as  $\Omega = \bigcup_{\forall i}^{Nel} \Omega_i$  such that  $\Omega_i \cap \Omega_j = \emptyset, \forall i \neq j$

Weak MRSU formulation starts with equation (4) in conservation form. Defining the suitable test and trial functions as

$$\mathcal{V}^h = \{N^h \in \mathcal{H}^1(\Omega) \text{ and } N^h = 0 \text{ on } \Gamma_D\}$$

$$\mathcal{S}^h = \{f^h \in \mathcal{H}^1(\Omega) \text{ and } \mathbf{F}^h = \mathbf{F}_D^h \text{ on } \Gamma_D\}$$

the weak formulation is written as, find  $\mathbf{F}^h \in \mathcal{S}^h$  such that  $\forall N^h \in \mathcal{V}^h$

$$\begin{aligned} \int_{\Omega} N^h \cdot \left( \frac{\partial \mathbf{F}^h}{\partial t} + \frac{\partial (\Lambda_i \mathbf{F})^h}{\partial x_i} \right) d\Omega + \sum_{e=1}^{Nel} \int_{\Omega_e} \left[ \sum_i \tau_i \Lambda_i \frac{\partial N^h}{\partial x_i} \right] \cdot \left( \frac{\partial (\Lambda_i \mathbf{F})^h}{\partial x_i} \right) d\Omega \\ + \sum_{e=1}^{Nel} \int_{\Omega_e} \delta^e \left( \frac{\partial N^h}{\partial x_i} \cdot \frac{\partial \mathbf{F}^h}{\partial x_i} \right) d\Omega = 0 \end{aligned}$$

where  $\tau_i = \frac{1}{\mathcal{D}|\Lambda_i|} \frac{1}{\sqrt{\mathcal{D}}} \left| \frac{\partial \mathbf{x}}{\partial \mathbf{r}} \right|$  with  $\mathcal{D}$ ,  $\mathbf{x}$  and  $\mathbf{r}$  being dimension, physical coordinates and natural coordinates respectively.  $\delta^e$  is the shock capturing parameter which will be defined later. First term is a standard Galerkin approximation. In the second expression, term inside square bracket is the enriched part of the test space which gives required diffusion. The last term is a shock capturing term which is used only for multidimensional problems and will be activated near in the high gradient region.

By taking moments one can obtain

$$\int_{\Omega} N^h \cdot \left( \frac{\partial P\mathbf{F}^h}{\partial t} + \frac{\partial P(\Lambda_i \mathbf{F})^h}{\partial x_i} \right) d\Omega + \sum_{e=1}^{Nel} \int_{\Omega_e} P \left[ \sum_i \tau_i \Lambda_i \frac{\partial N^h}{\partial x_i} \right] \cdot \left( \frac{\partial (\Lambda_i \mathbf{F})^h}{\partial x_i} \right) d\Omega + \sum_{e=1}^{Nel} \int_{\Omega_e} \delta^e \left( \frac{\partial N^h}{\partial x_i} \cdot \frac{\partial P\mathbf{F}^h}{\partial x_i} \right) d\Omega = 0 \quad (6)$$

The moments are given as

$$P\mathbf{F}^h = U^h, \quad P\Lambda_i \mathbf{F}^h = G_i^h$$

The domain boundary  $\Gamma$  is decomposed as

$$\Gamma = \overline{\Gamma_D} \cup \overline{\Gamma_N}, \quad \text{and } \overline{\Gamma_D} \cap \overline{\Gamma_N} = \emptyset$$

where  $\Gamma_D$  and  $\Gamma_N$  represents Dirichlet and Neumann boundaries.

As discussed in the introduction part, the weak formulation of (4) is started in conservation form. For stabilizing the algorithm only test space of convection part of the governing equation is enriched. Exact stabilization matrices are obtained for both scalar as well as vector conservation laws. In the above weak formulation group discretization of flux vector which are shown to be more accurate is used. Group discretization was first used in [41, 42] which was later extended for FEM based flux corrected transport schemes for multidimensional conservation laws by [43, 44]. In SUPG scheme these are used by [45] which shows improvement in the accuracy of the solution.

Now lets evaluate coefficients of diffusion as well as cross-diffusion matrices given by second term in equation (6).

### 7.1. One Dimensional Equation(s)

For two discrete velocity model

$$P \operatorname{sgn}(\Lambda) \Lambda \mathbf{F} = \lambda U$$

and for three discrete velocity model (including one rest particle)

$$P \operatorname{sgn}(\Lambda) \Lambda \mathbf{F} = \frac{2}{3} \lambda U$$

Hence, for one dimensional relaxation system three discrete velocity model is less diffusive which will be used for solving 1D problems.

### 7.2. Two Dimensional Equation(s)

Table 2 shows the expressions for diffusion as well as cross-diffusion vectors for various symmetric models.

Symmetric Model	$P \operatorname{sgn}(\Lambda_1) \Lambda_1 \mathbf{F}$	$P \operatorname{sgn}(\Lambda_1) \Lambda_2 \mathbf{F}$	$P \operatorname{sgn}(\Lambda_2) \Lambda_1 \mathbf{F}$	$P \operatorname{sgn}(\Lambda_2) \Lambda_2 \mathbf{F}$
$\mathcal{D}4$	$\lambda_1 U$	0	0	$\lambda_2 U$
$\mathcal{A} \mathcal{D}9$	$\frac{2}{3} \lambda_1 U$	0	0	$\frac{2}{3} \lambda_2 U$
$\mathcal{A}4$	$\frac{1}{2} \lambda_1 U$	0	0	$\frac{1}{2} \lambda_2 U$

Table 2: Diffusion and cross-diffusion vectors for symmetric models.

Firstly, it can be seen that the diffusion vectors are proportional to  $\lambda$ 's which are nothing but the supremum eigenvalues of the Jacobian matrices. One can use the  $\lambda$  as the global supremum eigenvalue but it produces excessive diffusion which smears the discontinuities. To reduce this diffusion a local supremum eigenvalue of the Jacobian

matrix is used. Second observation from the above diffusion expression is, among all two dimensional symmetric relaxation system models,  $\mathcal{A}4$  model gives less diffusion, hence hereafter, we shall use this model for all the computations.

**Remark:** One can easily show that the cross-diffusion vectors  $P \operatorname{sgn}(\Lambda_1)\Lambda_2\mathbf{F}$  and  $P \operatorname{sgn}(\Lambda_2)\Lambda_1\mathbf{F}$  vanishes in all symmetric models. These vectors are non-zero only in asymmetric models.

## 8. Temporal Discretization

For temporal discretization of semi-discrete scheme, forward Euler time discretization is used which can be obtained using Taylor series approximation in time about  $U^n$

$$U^{n+1} = U^n + \frac{\partial U^n}{\partial t} \Delta t + \frac{\partial^2 U^n}{\partial t^2} \frac{\Delta t^2}{2} + O(\Delta t^3)$$

where  $\Delta t = t^{n+1} - t^n$ . From which forward Euler time discretization can be obtained as

$$\frac{\partial U^n}{\partial t} = \frac{U^{n+1} - U^n}{\Delta t} + O(\Delta t)$$

The fully discretized nonlinear equations are linearized using Picard iteration and the corresponding system of equations are solved using Generalized Minimal Residual (GMRES) method.

## 9. Shock Capturing Parameter

In case of multidimensional MRSU method, diffusion along streamline direction is not sufficient to suppress the oscillations near high gradient regions. Hence additional diffusion terms with a shock capturing parameter is required which can sense these high gradient regions and add additional diffusion. There are many shock capturing parameters available in the literature [6, 7]. In this work we present a simple gradient based shock capturing parameter as follows.

We define a simple element-wise gradient based shock capturing parameter  $\delta^e$  which introduces diffusion along high gradient direction. Figure 3 (a) shows a typical four node quadrilateral element. As shown in figure, the maximum change in  $\Phi$  (where  $\Phi$  could be density, temperature, pressure or even water height (in case of shallow water equations); in present work, density is used for Euler test cases because density is the only primitive variable which jumps across all the three waves: shocks, expansion waves and contact discontinuities) occurs across node 1 and 3. The element based shock capturing parameter is then defined for node 1 and 3 as

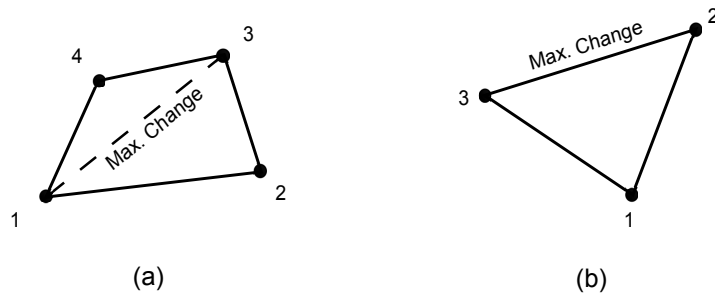


Figure 3: Four node quadrilateral element in physical domain

$$\delta_{1,3}^e = \frac{1}{\mathcal{D} \sqrt{\mathcal{D}}} \left| \frac{\partial \mathbf{x}}{\partial \mathbf{r}} \right| \left( \frac{\|\nabla \Phi\|_\infty^e}{\|\Phi\|_\infty^e} \right)$$

where subscripts 1 and 3 represent node numbers. For nodes 2 and 4, it is defined as

$$\delta_i^e = \frac{1}{\mathcal{D} \sqrt{\mathcal{D}}} \left| \frac{\partial \mathbf{x}}{\partial \mathbf{r}} \right| \left( \frac{\Phi_{\text{Max}}^e - \Phi_i^e}{\|\Phi\|_\infty^e} \right) \text{ where } i = 2, 4.$$

At element level matrix form, the shock capturing parameter is given by

$$\delta^e = \begin{bmatrix} \delta_1^e & 0 & 0 & 0 \\ 0 & \delta_2^e & 0 & 0 \\ 0 & 0 & \delta_3^e & 0 \\ 0 & 0 & 0 & \delta_4^e \end{bmatrix}$$

The upper and lower bound on the value  $\|\nabla\Phi\|_\infty^e$  is given by

$$0 \leq \|\nabla\Phi\|_\infty^e \leq \|\Phi\|_\infty^e$$

It is important to note that, the addition of extra shock capturing term in the weak formulation makes the formulation inconsistent with the original equation. Thus, we define  $\delta^e$  such that as element size  $\partial\mathbf{x} \rightarrow 0$ ,  $\delta^e$  should disappear. This condition is achieved by including  $\partial\mathbf{x}$  in the numerator, which vanishes as we refine the mesh. Similarly, one can define such a delta parameter for triangular elements shown in figure 3 (b).

The function of shock capturing parameter defined above is to add more diffusion in high gradient regions which is similar to that of limiter used in finite volume framework. Such schemes are known as high resolution schemes. High resolution schemes were first developed in finite difference framework [38]. A detailed description of these schemes is given in [39]. These schemes are essentially based on Godunov Order Barrier theorem [40] which says that, all monotone linear schemes are necessarily first order accurate and thus higher order approximation produces the spurious oscillation. High resolution schemes give accurate solution by suppressing these spurious oscillations caused due to higher order approximations. High resolution methods uses Flux / Slope limiters for switching from higher order accurate approximation to first order approximation near high gradients. These are also called Total Variation Diminishing (TVD) schemes. TVD schemes are also used in finite element framework [44].

### 9.1. Freezing of $\delta$

Calculation of  $\delta$  at every time step can be computationally expensive. Moreover, it can be shown that it stagnate the convergence of the scheme [49]. The remedy to this problem is to freeze  $\delta$  values if there is little difference in the successive residual values i.e., if

$$|\text{RES}(\text{current}) - \text{RES}(\text{previous})| < \text{Tol}$$

where RES and Tol are residual and desired tolerance value. This procedure results in the stagnation free convergence. Further, this procedure can be used for both steady state and transient problems.

## 10. Spectral Stability Analysis

Stability analysis of an explicit numerical scheme gives critical time step  $\Delta t_{cr}$  within which the scheme is stable. In other words, error in the solution does not grow with time. There are various methods available in the literature like von-Neumann and Spectral stability analysis. Unlike von-Neumann stability analysis, spectral stability analysis includes the boundary points too and hence more accurate than that of von-Neumann analysis. In this section a spectral stability analysis of MRSU scheme is done using one dimensional MRSU scheme for linear convection equation which is written as

$$\frac{u^{n+1}}{u^n} = \left[ I - M^{-1} \Delta t \left( Cc + \frac{\tilde{h}}{2} D\lambda \right) \right] = \mathcal{A}$$

where  $M, C$  and  $D$  are mass, convection and diffusion matrices given as

$$M = \int_{\Omega} (N^h)^T N^h d\Omega, \quad C = \int_{\Omega} (N^h)^T \left( \frac{dN^h}{dx} \right) d\Omega, \quad D = \int_{\Omega} \left( \frac{dN^h}{dx} \right)^T \left( \frac{dN^h}{dx} \right) d\Omega$$

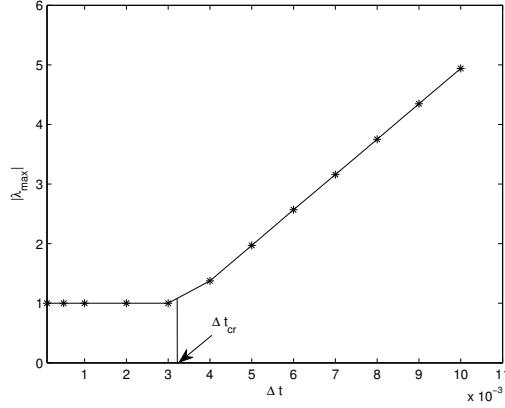


Figure 4: Critical time step vs. spectral radius.

$c, \tilde{h}$  are the constant wave speed and element length respectively. Matrix  $\mathcal{A}$  is an amplification matrix. The error at  $n^{th}$  time step  $\mathcal{E}^n = u_{exact} - u^n, \forall n \in \mathbb{R}^+$  also satisfies above equation, then

$$\frac{\mathcal{E}^{n+1}}{\mathcal{E}^n} = \mathcal{A}$$

For numerical stability error should not grow in time which gives

$$\left| \frac{\mathcal{E}^{n+1}}{\mathcal{E}^n} \right| \leq 1 \Rightarrow \|\mathcal{A}\| \leq 1 \Rightarrow |\varrho(\mathcal{A})| \leq 1$$

where  $\varrho(\mathcal{A}) \in \tilde{\sigma}(\mathcal{A})$  is the spectral radius of the amplification matrix. After simplification the critical time step is obtained as

$$\Delta t_{cr} \leq \frac{1}{\varrho\left(\frac{I}{\Delta t} - M^{-1}\left[Cc + \frac{\tilde{h}}{2}D\lambda\right]\right)} \quad (7)$$

Equation (7) gives an implicit expression for the critical time step.

As an example, linear convection equation (with unity wavespeed) is taken with cosine pulse as an initial condition given by equation (8) which is simply convecting in the domain  $[0, 1]$ .

$$u(x, 0) = \begin{cases} \frac{1}{2} \left(1 + \cos\left[\frac{\pi(x-0.2)}{0.12}\right]\right) & \text{for } |x - 0.2| \leq 0.12 \\ 0 & \text{Otherwise} \end{cases} \quad (8)$$

The spectral radius of amplification matrix  $|\lambda_{max}|$  is computed numerically with 50 node points. Figure 4 shows the  $\Delta t$  vs. spectral radius of amplification matrix. The critical value of time step is around  $3.2 \times 10^{-3}$ .

## 11. Numerical Experiments

In this section various 1D and 2D test cases are solved for Burgers equation, Euler and shallow water equations which shows the accuracy, robustness of the proposed scheme. These are the standard test cases which are chosen based on the complexity of the solution. Moreover, few new test cases for two dimensional problems are also introduced.

**Remark 1:** Residue plots are given for many steady state test cases where residue is calculated using relative  $\mathcal{L}_2$  error as

$$\text{Residue} = \frac{\|U^{n+1} - U^n\|_{\mathcal{L}_2}}{\|U^{n+1}\|_{\mathcal{L}_2}}$$

**Remark 2:** Full Gauss-quadrature integration rule is used for linear elements in 1D as well as in both four node quadrilateral (Q4) and three node triangular (T3) linear elements in 2D.

### 11.1. Error Analysis using 1D Convection Equation

Linear Lagrange interpolation function is used as a basis function in space. Experimental Order of Convergence (EOC) is calculated for a one dimensional convection equation with initial condition as a cosine wave (equation (8)) convecting with unity wave speed using  $\mathcal{L}_2$  and  $\mathcal{H}_1$  norm. Table 3 shows the EOC which is optimal for linear interpolation function  $N^h \in C^0(\Omega)$ .

No. of Nodes	$\mathcal{L}_2$	EOC	$\mathcal{H}_1$	EOC
40	0.1348	-	3.2934	-
80	0.0809	0.7366	2.1803	0.5951
160	0.0451	0.8430	1.3226	0.7211
320	0.0240	0.9101	0.7521	0.8144
640	0.0123	0.9644	0.4134	0.8634
1280	0.00615	1.0000	0.2195	0.9133
2560	0.00302	1.0260	0.1154	0.9276

Table 3: Convergence analysis of MRSU scheme.

### 11.2. 1-D Inviscid Burgers Test Cases with Smooth and Discontinuous Initial Data

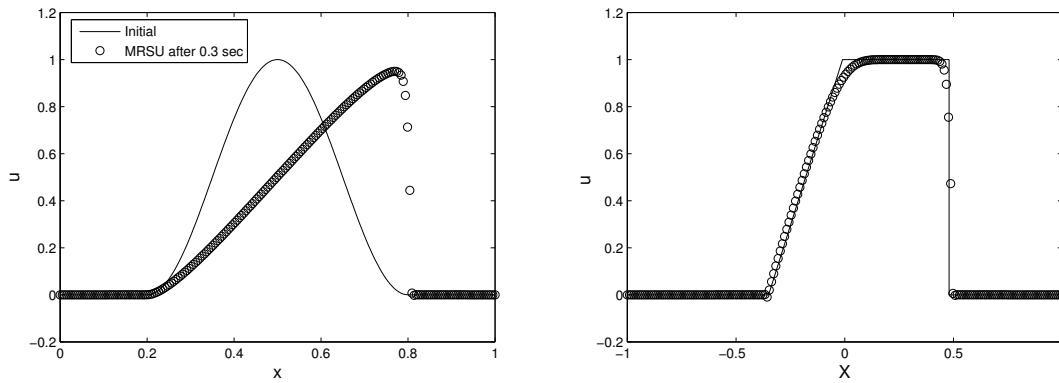


Figure 5: One-dimensional Burgers equation using MRSU.

The domain is  $[0, 1]$ . Number of node points are 200

$$\frac{\partial u}{\partial t} + \frac{\partial u^2/2}{\partial x} = 0$$

with initial condition as a cosine wave. Initial condition is

$$u(x, 0) = \begin{cases} \frac{1}{2} \left( 1 + \cos \left[ \frac{\pi(x-0.5)}{0.3} \right] \right) & \text{for } |x - 0.5| \leq 0.3 \\ 0 & \text{Otherwise} \end{cases}$$

Final time is  $t = 0.3$ ,  $CFL = 0.5$ .

The discontinuous initial condition is represented by a square wave as

$$u(x, 0) = \begin{cases} 1 & \text{for } |x| < 1/3 \\ 0 & \text{for } 1/3 < |x| \leq 1 \end{cases}$$

In both cases final time is  $t = 0.3$ ,  $CFL = 0.5$ . Figure 5 (left) shows smooth initial profile (solid line) and MRSU solution after 0.3 seconds with circles. Figure 5 (right) shows discontinuous exact solution (solid line) and MRSU solution (circles).

### 11.3. Sod's Shock Tube Problem [29]

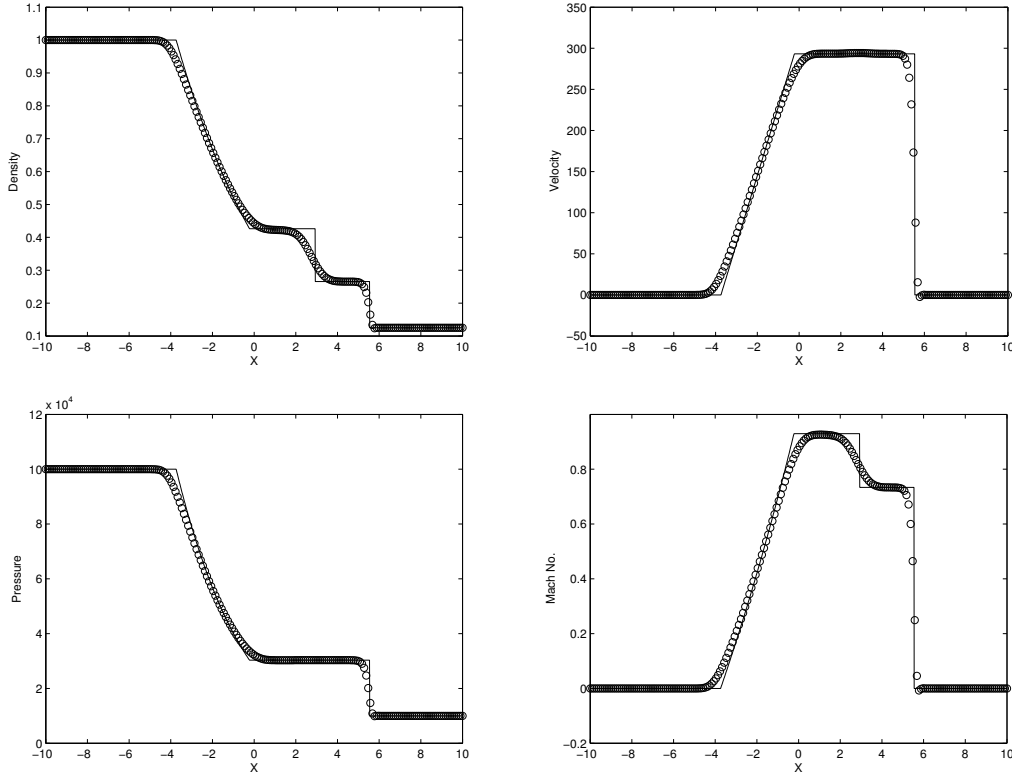


Figure 6: Density, velocity, pressure and Mach number plot using 200 nodes

The domain is  $[-10, 10]$ . Sod's shock tube problem consists of a left rarefaction, a right shock wave and a contact discontinuity which separates the rarefaction and shock wave. The initial conditions are given by

$$\rho(x, 0), u(x, 0), p(x, 0) = \begin{cases} 1, 0, 100000 & \text{If } -10 < x < 0 \\ 0.125, 0, 10000 & \text{If } 0 < x < 10 \end{cases}$$

The number of node points are 200 and CFL number is 0.2. Final time is  $t = 0.01$ . Figure 6 shows the density, velocity, pressure and Mach number plots. The solid line represent the exact solution while the circles are the numerical solution. Here, all the essential features like expansion wave, contact discontinuity and shock wave are captured reasonably well.

### 11.4. Shock-Entropy Wave Interaction [36]

In this test case a moving shock wave with Mach number 3 interacts with sinusoidal density profile. The domain is  $[0, 10]$ . The initial conditions are given as

$$(\rho, u, p)(x, 0) = \begin{cases} (3.857, 2.629, 10.3333) & \text{for } x < 1 \\ (1 + 0.2 \sin(5x), 0, 1) & \text{for } x \geq 1 \end{cases}$$

Final time is 1.8. No. of nodes used are 1000 and CFL no. is 0.4. This test case involve both shock wave and smooth profile. MRSU solution (represented by star) is compared with reference solution (solid line).

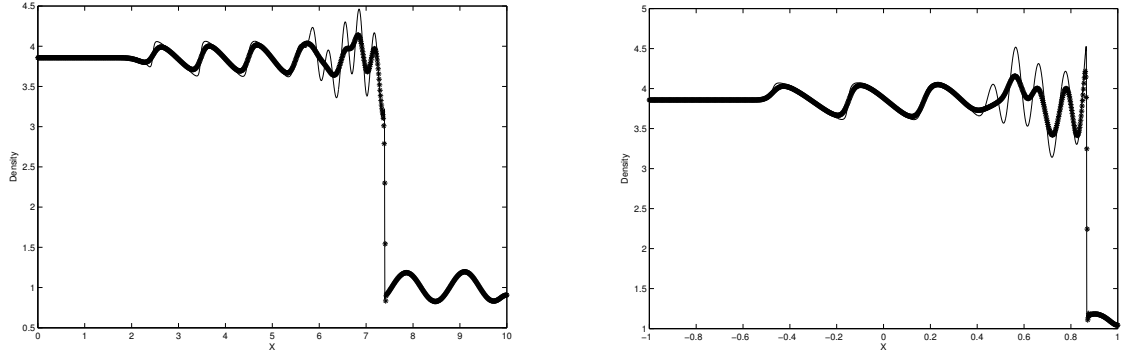


Figure 7: Density plots for shock-entropy waves interaction (right) and its variant (left).

Variant of this test case is also available which has a domain  $[-1, 1]$  and the initial conditions are

$$(\rho, u, p)(x, 0) = \begin{cases} (3.857, 2.629, 10.3333) & \text{for } x < -0.8 \\ (1 + 0.2 \sin(5\pi x), 0, 1) & \text{for } x \geq -0.8 \end{cases}$$

Final time is 0.47. No. of nodes used and CFL no. are same as above. The proposed scheme captures all the essential flow features of both the test cases as shown in figure 7.

#### 11.5. Woodward and Colella Blastwave Problem [64]

It is one of the severe test case used to test the robustness and accuracy of the numerical scheme. The domain is  $[0, 1]$ . The initial conditions are given as  $\rho = 1$  and  $u = 0$  everywhere in the domain. Pressure is given as

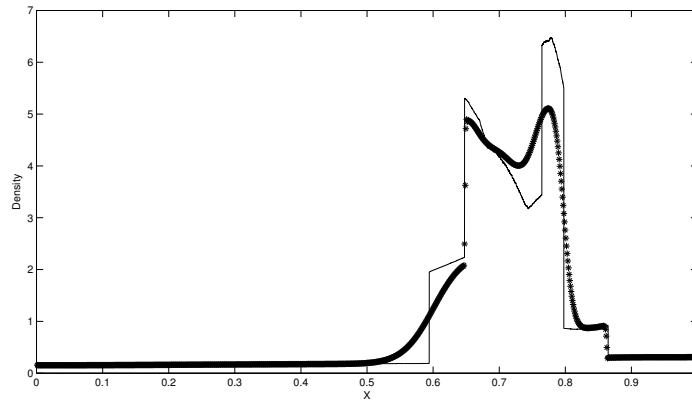


Figure 8: Density plot for blastwave problem with 1000 node points

$$p(x, 0) = \begin{cases} 1000 & \text{for } x \in [0, 0.1] \\ 0.01 & \text{for } x \in [0.1, 0.9] \\ 100 & \text{for } x \in [0.9, 1] \end{cases}$$

The final time is 0.038. The solution consist of interaction of strong expansion with strong shock and contact waves. MRSU (star) resolves all the flow features with just 1000 nodes as shown in figure 8. The reference solution (shown in solid line) is generated with 10000 nodes Random choice method.

### 11.6. Dam Break Problem [63]

Figure 9 shows the results of dam break problem. CFL = 0.25 , number of nodes = 200 and final time = 50 sec are used. MRSU scheme can capture all the flow features like expansion region and hydraulic jump reasonably well with such a crude grid shown by circles. The exact solution is given by solid line.

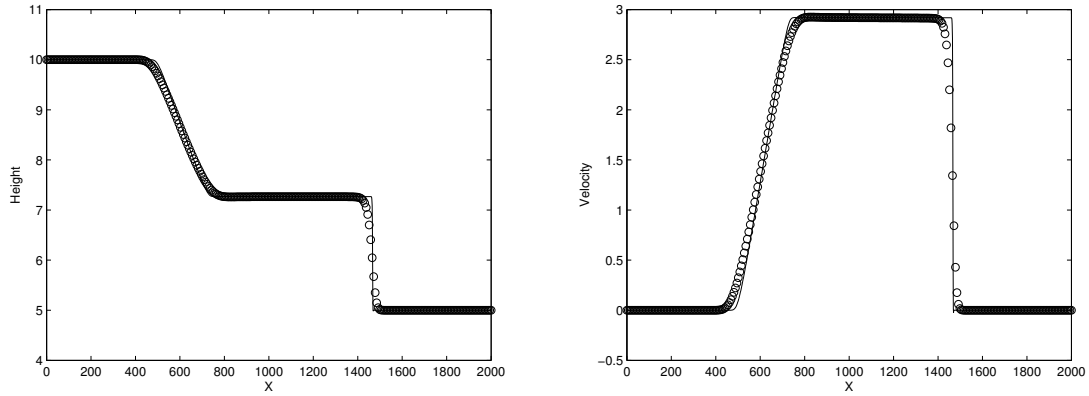


Figure 9: Height and velocity plots for dam break problem with 200 nodes.

### 11.7. Extreme Expansion Wave Problem [62]

In the simulation CFL = 0.3, number of nodes = 200 and final time = 20 sec are used. Figure 10 shows the results of extreme expansion wave problem. The expansion waves are captured correctly.

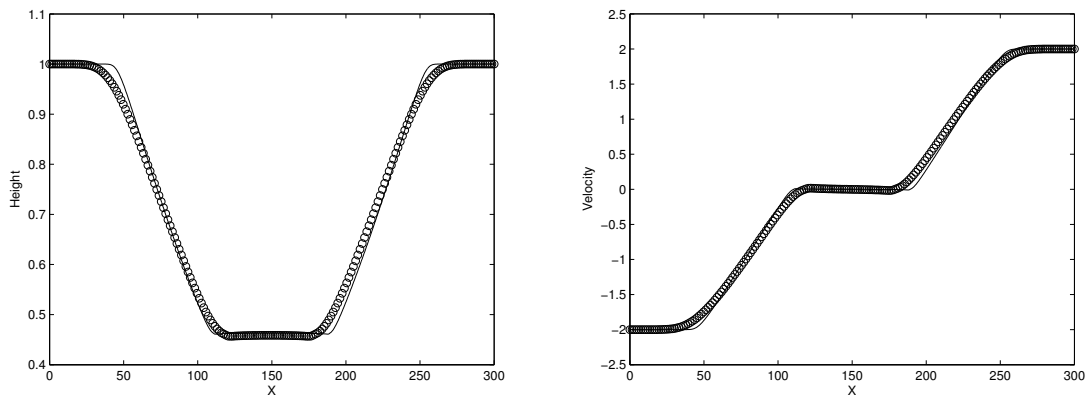


Figure 10: Height and velocity plots for extreme expansion wave problems with 200 nodes.

### 11.8. Strong Shock Problem [62]

Figure 11 shows the results of strong shock problem. In the simulation CFL = 0.4, number of nodes = 200, final time = 40 sec is used. MRSU scheme can capture discontinuous wavefronts reasonably well.

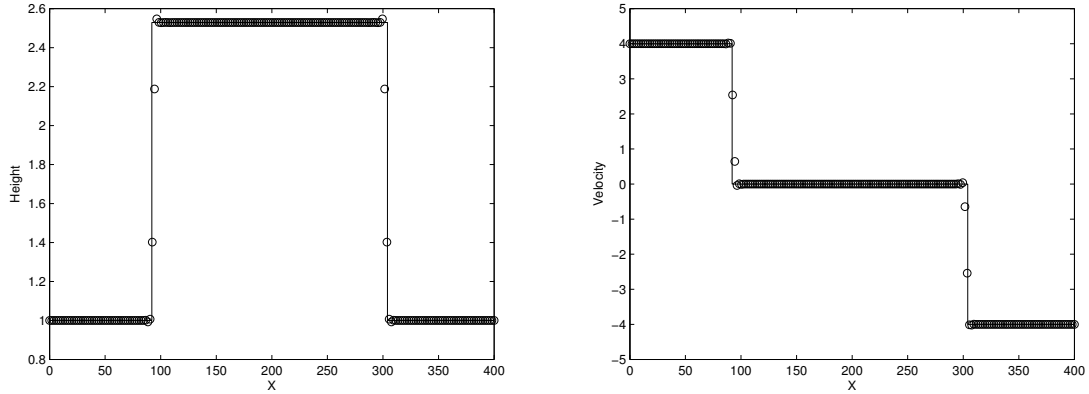


Figure 11: Height and velocity plots for strong shock problem with 200 nodes.

### 11.9. 2D Burgers Test Case 1

Two dimensional Burgers equations is given by

$$\frac{\partial u}{\partial t} + \frac{\partial \left( \frac{u^2}{2} \right)}{\partial x} + \frac{\partial u}{\partial y} = 0$$

The boundary conditions are:

$$u(0, y) = 1 \text{ and } u(1, y) = -1, \quad 0 < y < 1$$

and

$$u(x, 0) = 1 - 2x, \quad 0 < x < 1$$

Exact solution is given in [32]. The normal discontinuity is well captured using  $64 \times 64$  and  $128 \times 128$  grid as shown in figure 12.

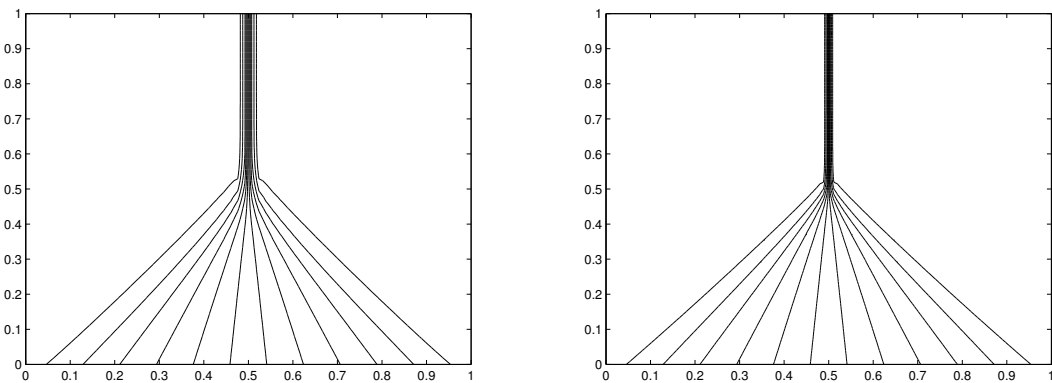


Figure 12:  $64 \times 64$  (left) and  $128 \times 128$  (right) quadrilateral mesh.

### 11.10. 2D Burgers Test Case 2

For two dimensional Burgers test case the boundary conditions are:

$$u(0, y) = 1 \text{ and } u(1, y) = -1, \quad 0 < y < 1$$

and

$$u(x, 0) = 1 - 2x, \quad 0 < x < 1$$

Exact solution is given in [32]. The oblique discontinuity is captured quite accurately as shown in figure 13 with different grid size.

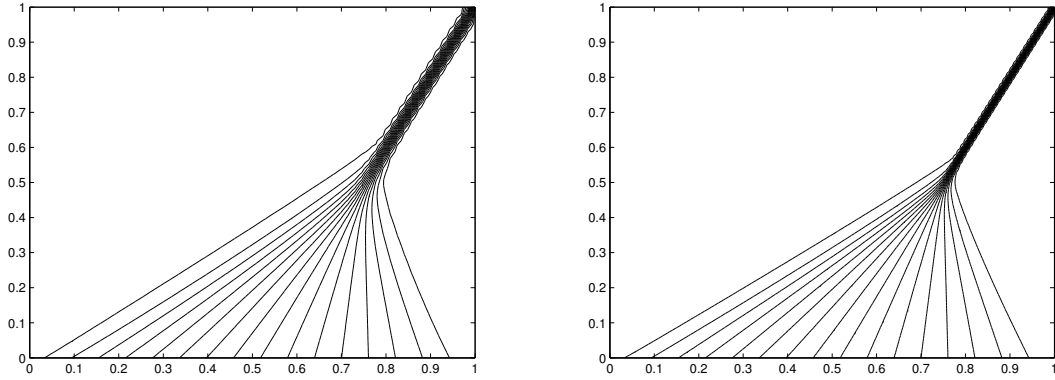


Figure 13:  $64 \times 64$  (left) and  $128 \times 128$  (right) quadrilateral mesh.

#### 11.11. 2D Burgers Test Case with Non-convex Flux Function -KKP Rotating Wave [37]

The domain is  $[-2, 2] \times [-2.5, 1.5]$ . The 2D scalar conservation law with non-convex flux function is

$$\frac{\partial u}{\partial t} + \frac{\partial \sin u}{\partial x} + \frac{\partial \cos u}{\partial y} = 0$$

with initial conditions as

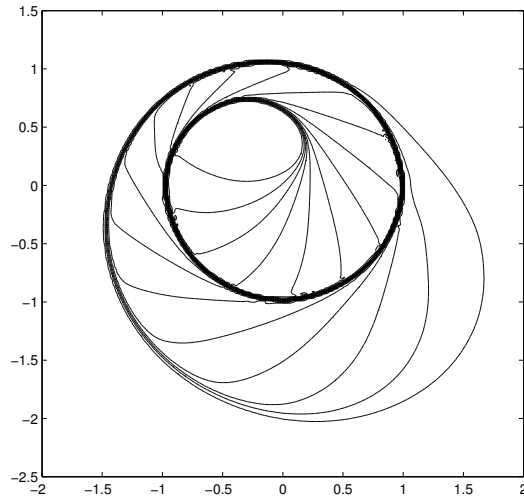


Figure 14: KKP rotating wave

$$u(x, y, 0) = \begin{cases} 3.5\pi & \text{If } x^2 + y^2 < 1 \\ \frac{\pi}{4} & \text{otherwise} \end{cases}$$

Figure 14 shows the contour plots on mesh  $\Delta x = \Delta y = 1/50$ .

### 11.12. Shock Reflection Test Case

In this test case [31] the domain is rectangular  $[0, 3] \times [0, 1]$ . The boundary conditions are, inflow (left boundary) :  $\rho = 1, u = 2.9, v = 0, p = 1/1.4$ . Post shock condition (top boundary) :  $\rho = 1.69997, u = 2.61934, v = -0.50633, p = 1.52819$ . Bottom boundary is a solid wall where slip boundary condition is applied, *i.e.*,  $\mathbf{v} \cdot \mathbf{n} = 0$ . At right boundary where the flow is supersonic all primitive variables  $\rho, u, v$  and  $p$  are extrapolated with first order approximation. Pressure plots for  $60 \times 20, 120 \times 40$  and  $240 \times 80$  quadrilateral mesh along with the comparison of residue plots are

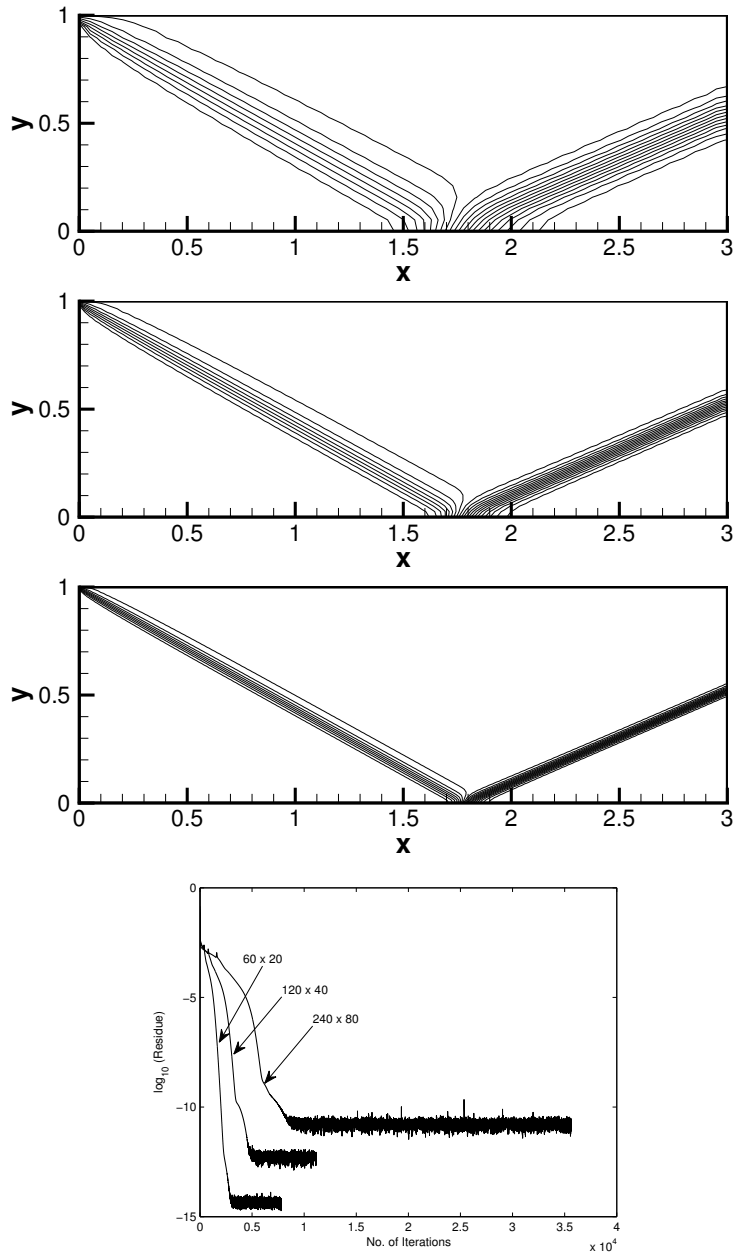


Figure 15: Pressure contours (0.8:0.1:2.8)  $60 \times 20, 120 \times 40$  and  $240 \times 80$  quadrilateral mesh using Q4 element. Residue plots are shown below.

given in figure 15.

### 11.12.1. Oblique Shock Reflection over a Unstructured Triangular Mesh

For triangular unstructured mesh (number of nodes: 2437 and number of triangles: 4680) the pressure contours are given in figure 16.

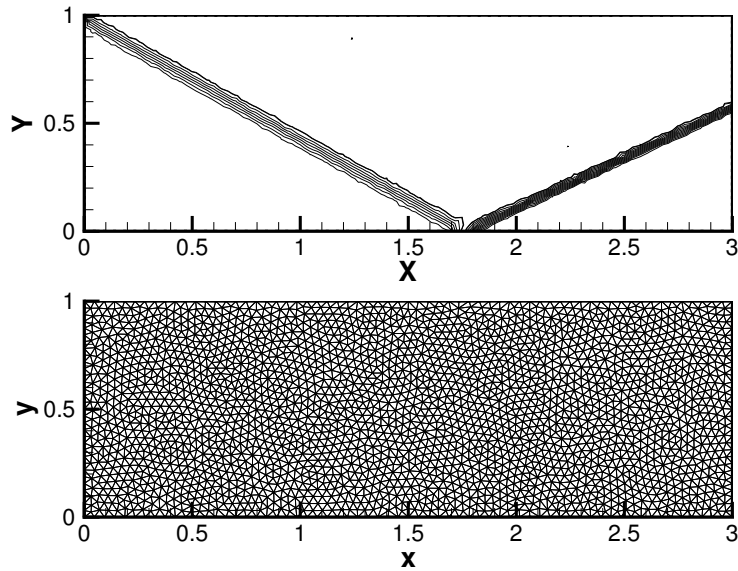


Figure 16: Pressure contours using T3 element.

### 11.13. Half Cylinder Test Case

Four supersonic test cases with inflow Mach numbers 2, 3, 6 and 20 are tested on a half cylinder [33]. The domain is half circular, the left outer circle is inflow boundary. Small circle inside the domain is a cylinder wall and the straight edges on right side are supersonic outflow boundaries. Pressure plots (see figure 17) shows that the bow

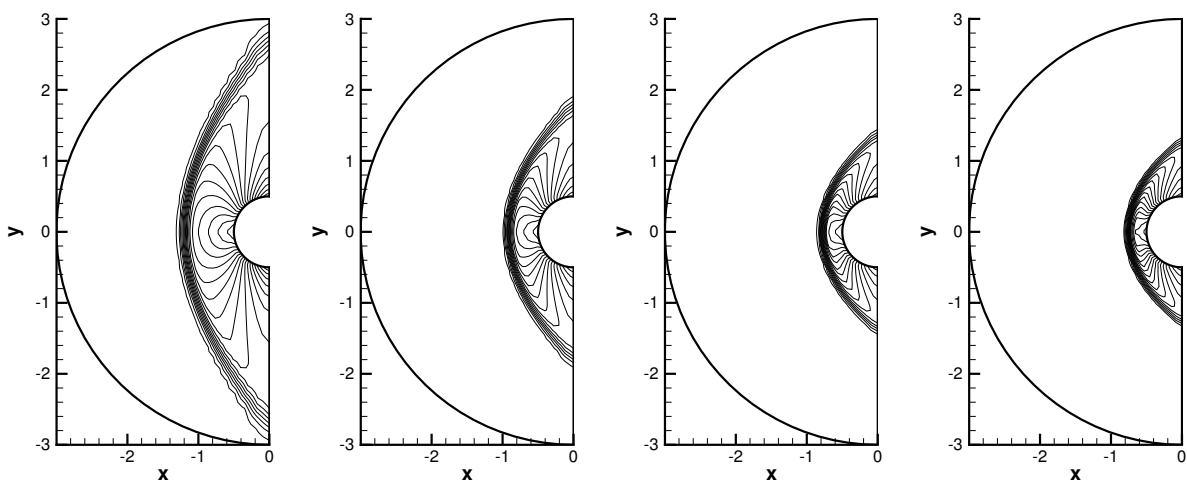


Figure 17: Pressure contours for Mach 2 (0.8:0.2:4), Mach 3 (1:0.5:16), Mach 6 (2:2:32) and Mach 20 (20:20:360) using  $46 \times 46$  quadrilateral mesh.

shock in front of the half-cylinder is captured accurately at the right position in each case which are compared with existing results [35].

#### 11.14. Double Mach Reflection Test Case

In the initial condition, the Mach 10 shock wave makes an angle of  $60^\circ$  with the reflecting wall. The undisturbed air in front of shock has density 1.4 and pressure 1. The initial conditions and boundary conditions are given in [64]. The triple point is formed where three shocks meet. Many schemes produce unphysical kinked Mach stem. MRSU

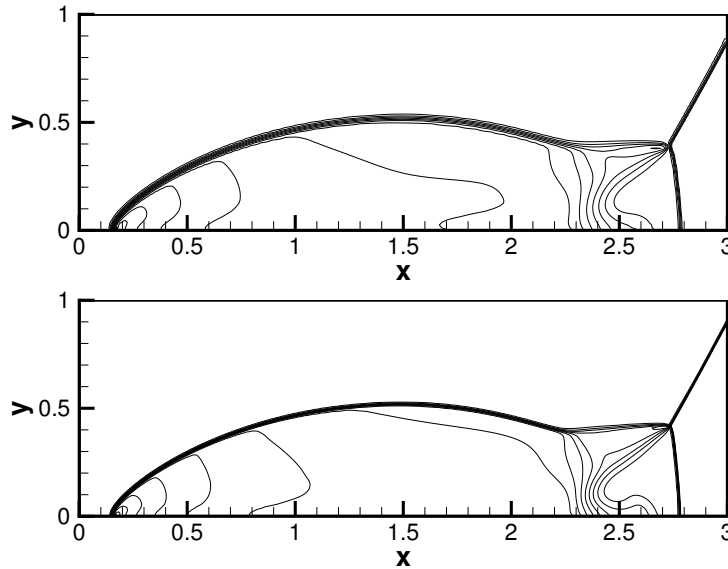


Figure 18: Density contours (3:0.92:26)  $240 \times 80$  (top) and  $480 \times 160$  (bottom) Q4 mesh

scheme accurately captures all the shock correctly without any kink in the Mach stem as shown in figure 18.

#### 11.15. $15^\circ$ Ramp Test Case

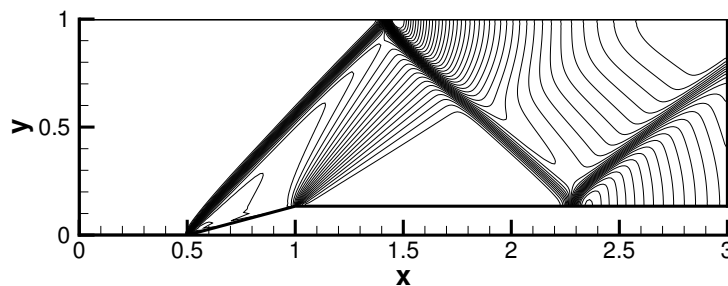


Figure 19: Pressure contours (0.8:0.05:2) for  $240 \times 80$  quadrilateral mesh using MRSU scheme.

In case of supersonic flow over a  $15^\circ$  ramp [34] the inlet (left boundary) Mach number is 2, top and bottom boundaries are inviscid walls and the outlet (right boundary) is supersonic. Oblique shock wave over a wedge hits the top wall and is reflected back. Expansion waves interact with this reflected shock which results in weakening of shock strength. This shock reflects again from the bottom boundary. Figure 19 shows the pressure plots for structured quadrilateral (Q4) mesh whereas figure 20 shows the pressure plots for unstructured triangular (T3) mesh.

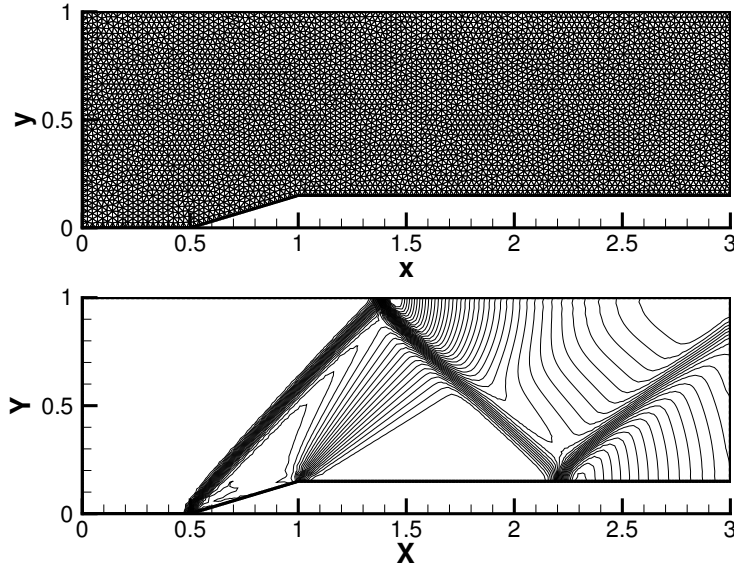


Figure 20: Triangular Mesh and pressure contours (0.8:0.05:2.8).

#### 11.16. Parallel Jet Flow [46]

The domain is  $[0, 1] \times [0, 1]$  and the initial condition is given as

$$\begin{aligned} M_1 &= 4, \rho_1 = 0.5, p_1 = 0.25 \text{ if } y > 0.5 \\ M_2 &= 2.4, \rho_2 = 1, p_2 = 1 \text{ if } y < 0.5 \end{aligned}$$

The boundary conditions are, left boundary is the supersonic inflow and top, right and bottom boundaries are supersonic outflow where all the variables are extrapolated. Figure 21 shows the density and pressure plots for  $51 \times 51$  and  $101 \times 101$  node points. All the flow features like shock, expansion and contact are resolved quite well using MRSU scheme.

#### 11.17. Modified Parallel Jet Flow

This is a slightly modified parallel jet flow test case which is used to demonstrate the capturing of contact wave when it is not aligned with the mesh. The domain is same but the initial condition is

$$\begin{aligned} M_1 &= 4, \rho_1 = 0.5, p_1 = 0.08 \text{ if } y > 0.5 \\ M_2 &= 2.8, \rho_2 = 1, p_2 = 1.3 \text{ if } y < 0.5 \end{aligned}$$

Boundary conditions are same as above. Figure 22 shows the density and pressure plots for  $51 \times 51$  and  $101 \times 101$  node points. The contact wave is captured well using MRSU scheme.

#### 11.18. Circular Explosion Problem[59]

In this test case the domain is  $[-1, 1] \times [-1, 1]$ . The initial conditions represents two regions. First is inside the circle with radius 0.4 and second region is outside that circle. The initial conditions are

$$(\rho, u, v, p)(x, y, 0) = \begin{cases} (1, 0, 0, 1) & \text{If } |r| \leq 0.4 \\ (0.125, 0, 0, 0.1) & \text{Otherwise} \end{cases}$$

The final time is 0.2. The solution has circular shock, constantly moving away from the center. The circular expansion fan is moving towards the center. All these features are well captured by MRSU scheme. Figure 23 shows the density, pressure and velocity in x and y direction contours. One can see the shock, contact as well as expansion wave in density contours, whereas, as expected only shock and expansion wave is present in the pressure contours.

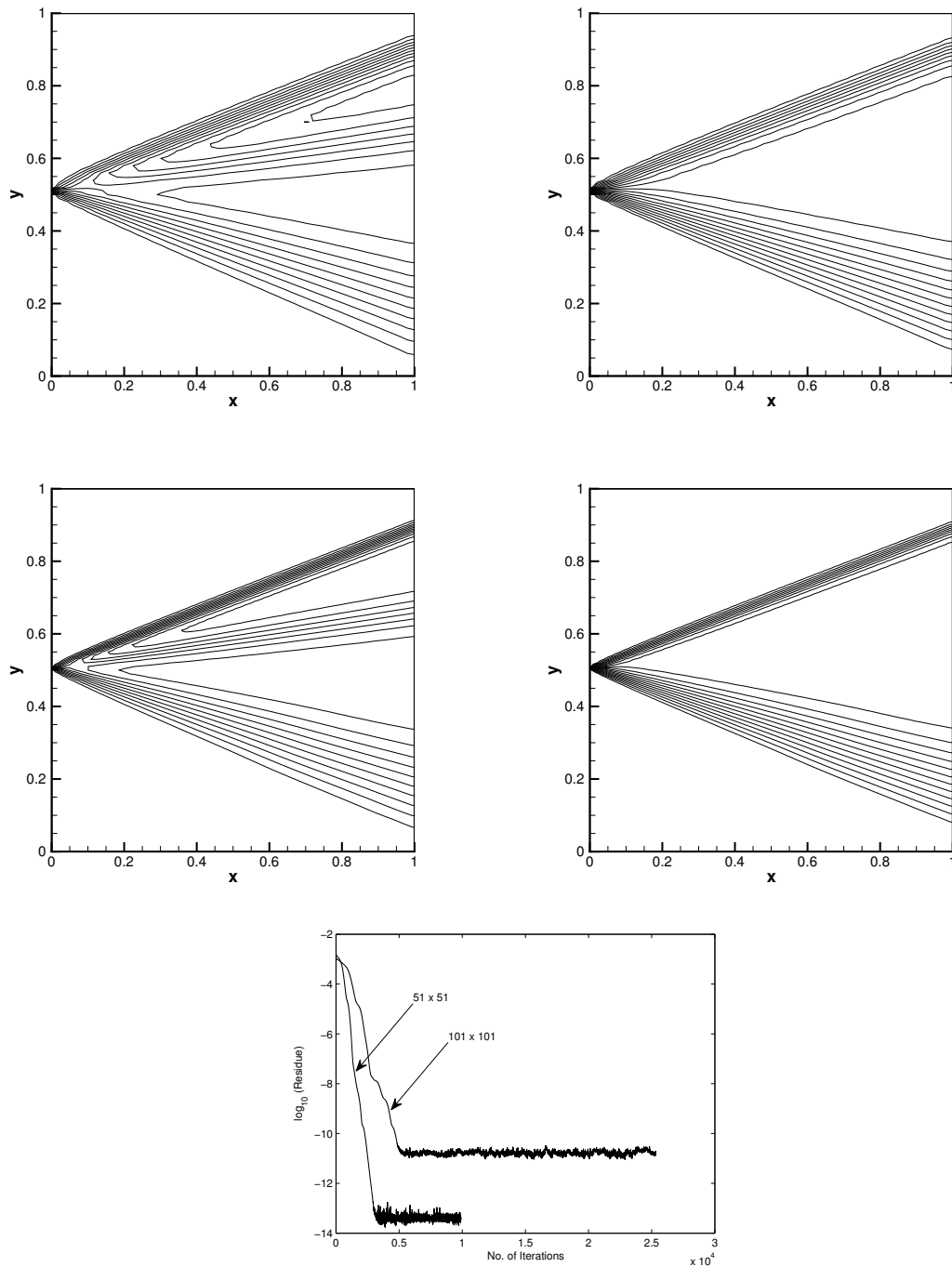


Figure 21: Density (0.55:0.03:0.94) (left) and pressure (0.3:0.03:0.9) (right) contours for  $51 \times 51$  (top) and  $101 \times 101$  (bottom) quadrilateral mesh. Residue plots are given for both the mesh.

### 11.19. Flow Over a Bump

The bump height is 4% of that of chord length. Here three different flow fields are considered, namely, Mach 0.5 (subsonic flow), Mach 0.85 (Transonic flow) and Mach 1.4 (Supersonic flow) over a Bump. Due to presence of

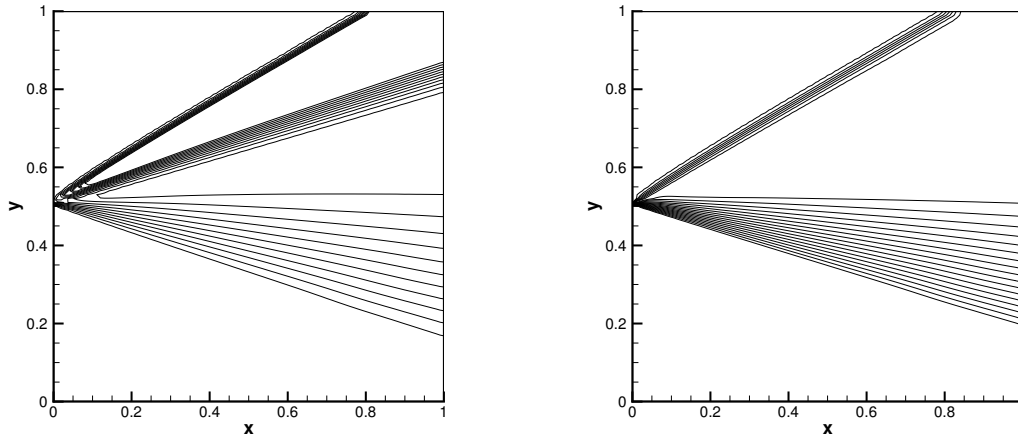


Figure 22: Density contours 0.42:0.048:0.9 (left) and pressure contours 0.05:0.04:1.05 (right) for  $101 \times 101$  quadrilateral mesh.

stagnation point at the front and rear end of the bump this test case becomes difficult to solve.

#### 11.19.1. Supersonic Flow with $M = 1.4$

Figure 24 shows the pressure contours for Mach 1.4. In this test case shock appears from the leading edge of the bump which hits the top wall and then reflects back towards bottom wall. The reflected shock interacts with the shock generated from the trailing edge of the bump and it reflects again from the bottom boundary. MRSU captures all the essential flow features accurately.

#### 11.19.2. Transonic Flow with $M = 0.85$

Figure 25 shows the pressure contours for Mach 0.85 and the variation of Mach number along the bottom wall. The shock appears approximately at 86% of the bump from the front with upstream Mach number approximately 1.3.

#### 11.19.3. Subsonic Flow with $M = 0.5$

In this case no shock wave appears. Figure 26 shows the pressure contours for Mach 0.5 and the variation of Mach number along the bottom wall. The change in Mach number along the bottom wall is small. It decreases at the front and rear stagnation points.

For both transonic as well as subsonic flow over the bump Riemann invariant based boundary conditions are used.

#### 11.20. Supersonic Flow Over a Reverse Bump

This is a new test case introduced here by reversing the bump. The inlet Mach number is 1.4. Expansion waves originates from the leading edge of the reverse bump. The curved surface of the reverse bump compresses the flow isentropically which generates Mach waves. The Mach waves coalesce to form an oblique shock at an angle of  $50^\circ$  approximately with the horizontal bottom wave which hits the inviscid top wall where no slip boundary conditions are applied. The incident shock wave reflects from the top wall. From the trailing edge of the reverse bump a second expansion wave originates which interacts with the reflected shock wave. The important features of this test case is to capture the shock wave and expansion waves correctly. Figure 27 shows the pressure contours on  $240 \times 80$  quadrilateral mesh.

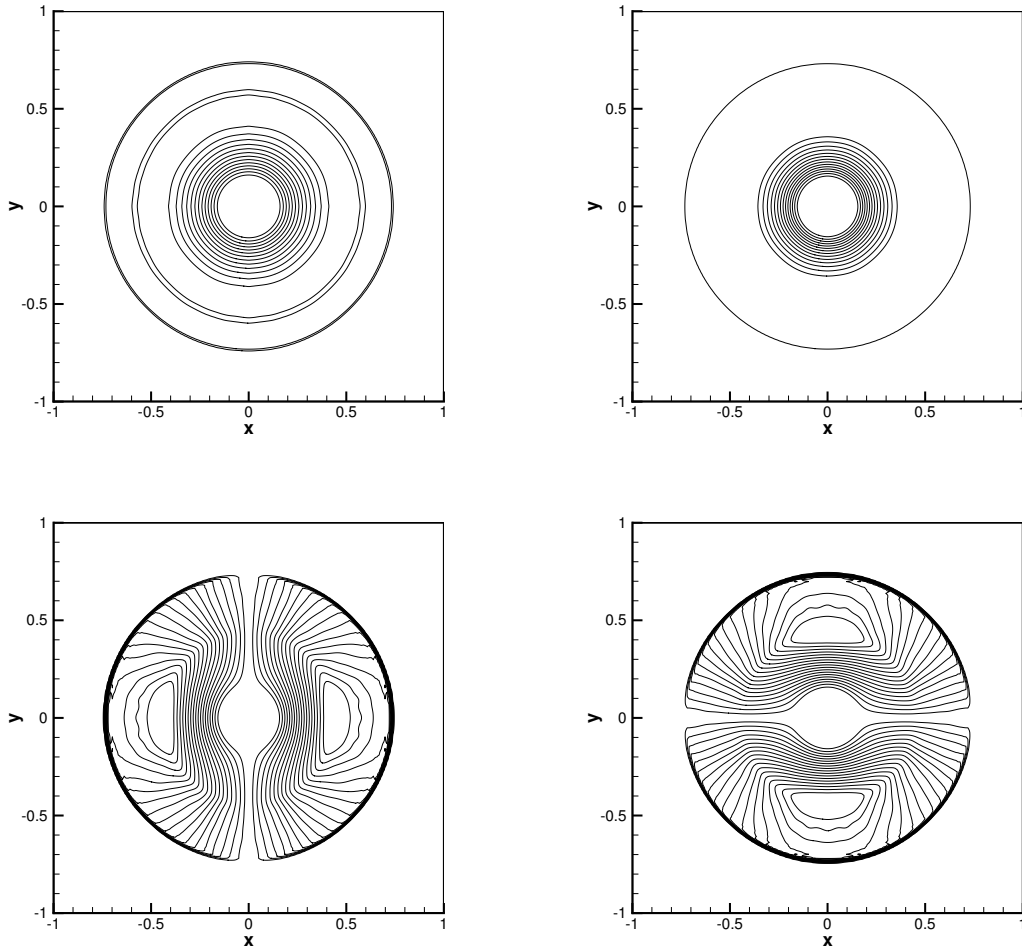


Figure 23: Density (0.22:0.042:0.86), pressure (0.2:0.05:0.95), velocity in X (-0.9:0.05:0.9) and Y (-0.9 : 0.05 : 0.9) direction contours using  $200 \times 200$  elements.

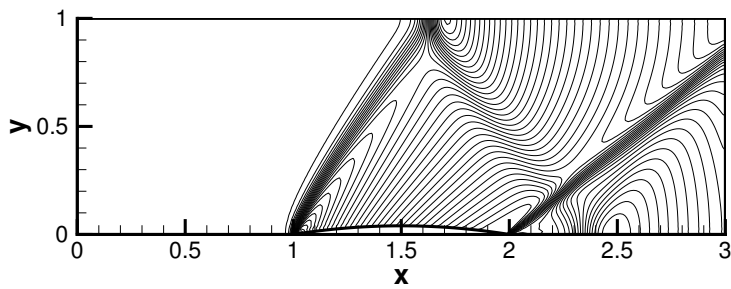


Figure 24: Mach 1.4 pressure contours (0.5:0.02:1.4) with  $240 \times 80$  quadrilateral mesh.

### 11.21. 2D Riemann Problems [60]

Three Riemann problems are consider here namely Case1, 2 and 3. Riemann problems are solved on domain  $[0, 1] \times [0, 1]$ . This square domain is divided in four quadrant where initial constant states are defined. These

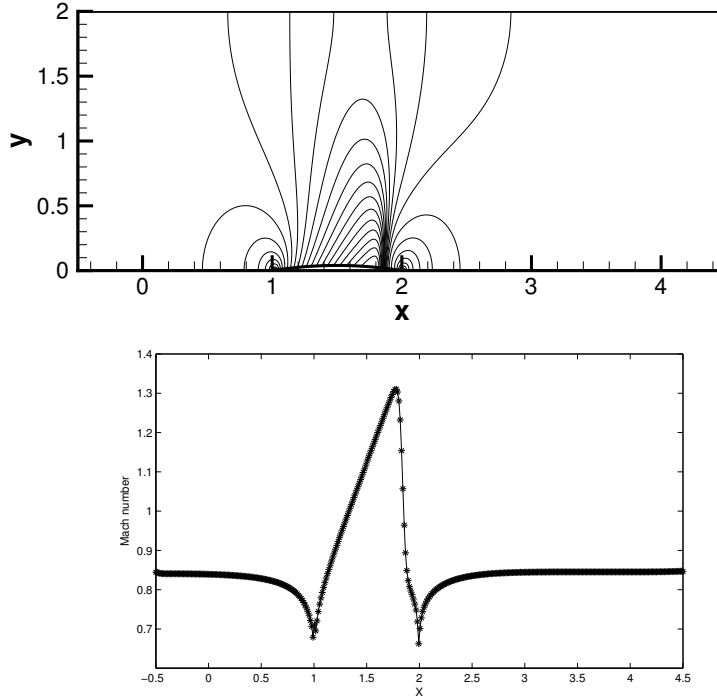


Figure 25: Mach 0.85 pressure contours (0.45:0.02:0.89) with  $400 \times 160$  quadrilateral mesh and Mach number variation along the bottom wall.

problems are proposed in such a way that the solution between these quadrant have only one wave like shock, contact etc. In both case 1 and 2 all the four waves are shock waves whereas in case 3 all waves are contact waves. The initial conditions for Case 1 is

$$(\rho, u, v, p)(x, 0) = \begin{cases} (1.1, 0, 0, 1.1) & x \geq 0.5 \text{ and } y \geq 0.5 \\ (0.5065, 0.8939, 0, 0.35) & x \geq 0.5 \text{ and } y < 0.5 \\ (0.5065, 0, 0.8939, 0.35) & x < 0.5 \text{ and } y \geq 0.5 \\ (1.1, 0.8939, 0.8939, 1.1) & x \leq 0.5 \text{ and } y \leq 0.5 \end{cases}$$

and for Case 2

$$(\rho, u, v, p)(x, 0) = \begin{cases} (1.5, 0, 0, 1.5) & x \geq 0.5 \text{ and } y \geq 0.5 \\ (0.5323, 1.206, 0, 0.3) & x \geq 0.5 \text{ and } y < 0.5 \\ (0.5323, 0, 1.206, 0.3) & x < 0.5 \text{ and } y \geq 0.5 \\ (0.138, 1.206, 1.206, 0.029) & x \leq 0.5 \text{ and } y \leq 0.5 \end{cases}$$

Finally, for Case 3 the initial conditions are

$$(\rho, u, v, p)(x, 0) = \begin{cases} (1, 0.75, -0.5, 1) & x \geq 0.5 \text{ and } y \geq 0.5 \\ (2, 0.75, 0.5, 1) & x \geq 0.5 \text{ and } y < 0.5 \\ (3, -0.75, -0.5, 1) & x < 0.5 \text{ and } y \geq 0.5 \\ (1, -0.75, 0.5, 1) & x \leq 0.5 \text{ and } y \leq 0.5 \end{cases}$$

Figure 28 and 29 shows the density contours for case 1, 2 and case 3 respectively.

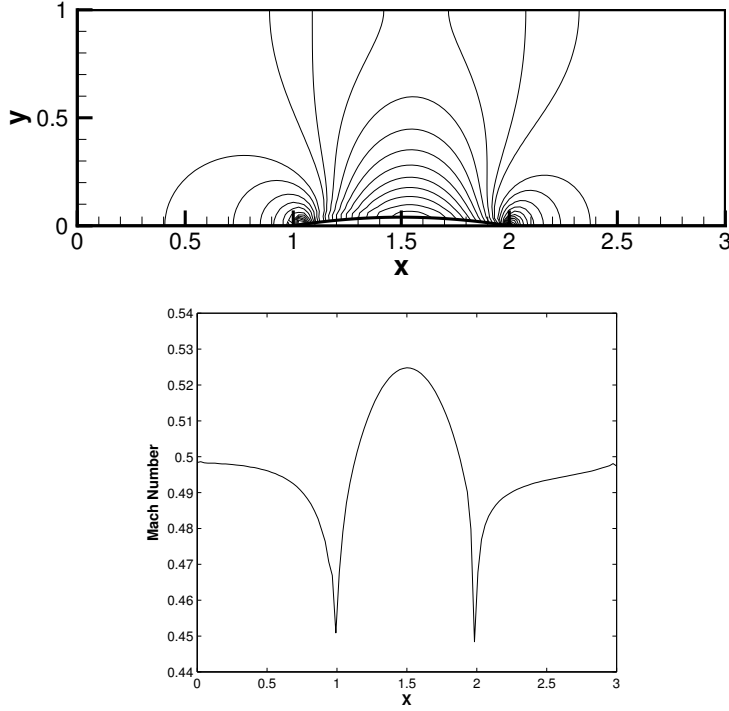


Figure 26: Mach 0.5 pressure contours (0.68:0.003:0.775) with  $120 \times 40$  quadrilateral mesh and Mach number variation along the bottom wall.

### 11.22. Circular Dam Break Test Case

In this test case the domain is  $[0, 1] \times [0, 1]$ . The circular dam is placed at the center. The initial water height is

$$h = \begin{cases} 2 & \text{If } x < 100m \\ 1 & \text{Otherwise} \end{cases}$$

and  $u = v = 0$ . All boundary conditions are transmissive. Sudden breaking of circular dam creates radially outward propagating hydraulic jump and radially inward propagating depression wave. These waves are captured well as shown in figure 30.

### 11.23. Hydraulic Jump [57]

This test case gives a hydraulic jump in a convergent wall section. In this case the flow is supercritical. The computational domain is  $[0, 40] \times [0, 30]$  and it is discretized using  $80 \times 60$  node points. The initial conditions are,  $h = 1m$ ,  $u = 8.57m/s$  and  $v = 0$ . The wall angle for the convergent section is  $8.95^\circ$ . The boundary conditions are reflective at top and bottom walls whereas supercritical boundary conditions are imposed on inflow and outflow boundary. Figure 31 shows the contours of height  $h$ . The hydraulic jump is captured very well with such a crude grid.

### 11.24. Hydraulic Jump Interaction in a Convergent Channel

This test case is a slight modification of previous test case where the walls are converging from both top and bottom with fixed angle  $8.95^\circ$  which form a convergent channel. Again, the flow is supercritical. The computational domain is  $[0, 50] \times [0, 30]$  and it is discretized using  $100 \times 60$  node points. The initial conditions are same as before. The boundary conditions are reflective at top and bottom walls whereas supercritical boundary conditions are applied on the inflow and outflow boundaries. Hydraulic jump generated from top and bottom wall intersects each other and then reflects from the top and bottom boundary. This interaction of hydraulic jump is captured well by MRSU scheme. Both contour plots for height and surface plots are given in figure 32.

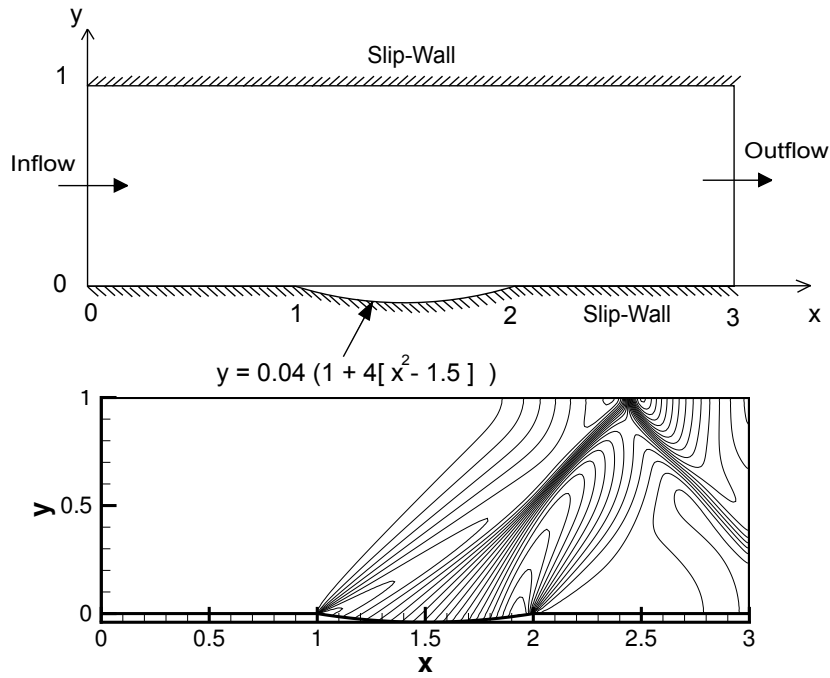


Figure 27: (Top) geometry of the reverse bump and (bottom) Mach 1.4 pressure contours (0.4:0.032:1.2) with  $240 \times 80$  quadrilateral mesh.

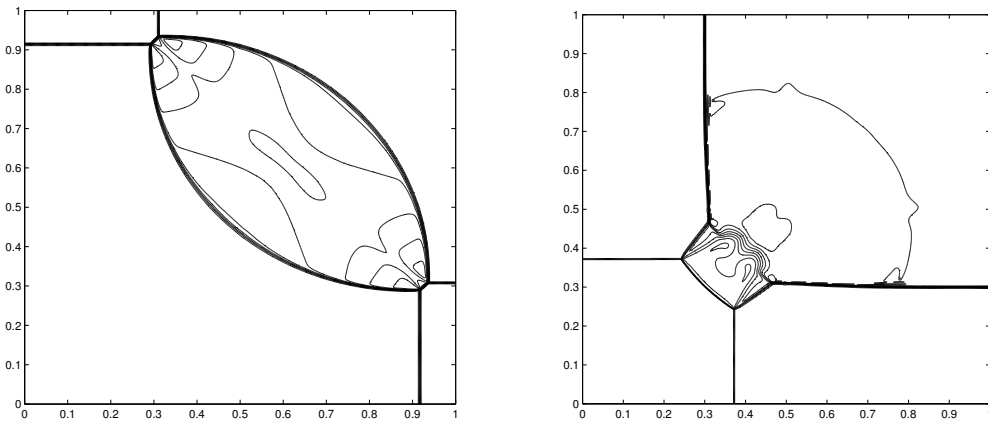


Figure 28: Density contours for 2D Riemann problem case 1 (left) and 2 (right) using  $400 \times 400$  mesh.

### 11.25. Partial Dam Break Test Case [57]

This is a 2D test case for shallow water flows which simulates the partial dam break due to sudden opening of sluice gate in a rectangular channel. The domain is  $[0, 200m] \times [0, 200m]$  and the length of sluice gate is 75m long as shown in first figure of 33. The initial condition is

$$h = \begin{cases} h_1 m & \text{If } x < 100m \\ h_2 m & \text{Otherwise} \end{cases}$$

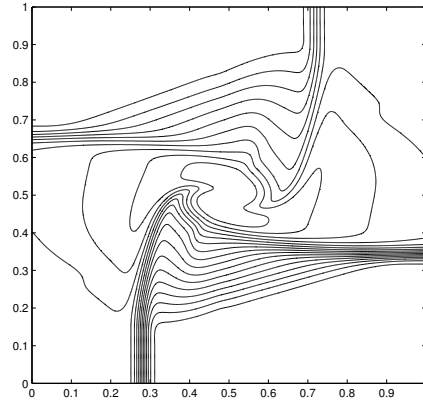


Figure 29: Density contours for 2D Riemann problem case 3 using  $400 \times 400$  mesh.

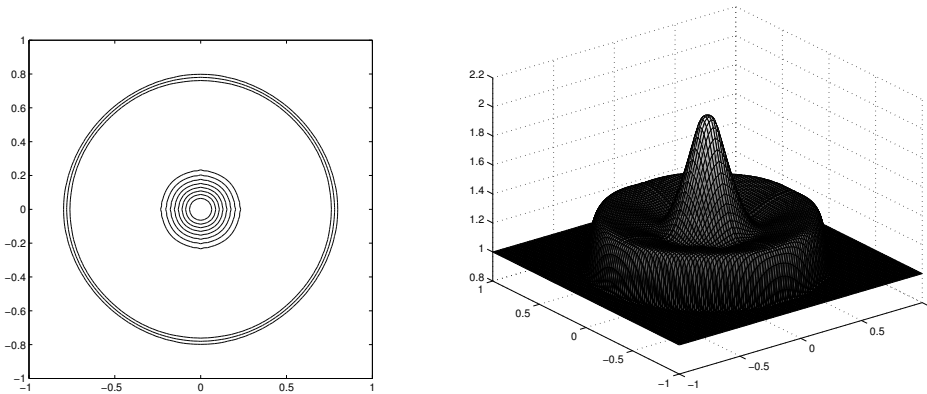


Figure 30: Dam break problem height contours (1.075:0.075:1.93) and surface plot on  $101 \times 101$  quadrilateral mesh.

and  $u = v = 0$ . Boundary conditions are transmissive on left as well as right boundary, whereas reflective boundary conditions are used for remaining boundaries. Strong bore in the upstream and negative waves in the downstream directions are created due to sudden opening of sluice gate. The solution is plotted at  $t = 7.2$  sec. The unstructured triangular mesh is used for the simulation, the number of nodes are 4238 and the number of elements are 8114. Second and third figure of 33 shows the contour with velocity vector plots and surface plot respectively.

## 12. Conclusions

A new stabilized finite element method, namely, Method of Relaxed Streamlined Upwinding (MRSU) scheme is proposed for hyperbolic conservation laws. There are several advantages of the proposed scheme.

1. MRSU gives exact diffusion vectors which is required for stabilization of the numerical scheme.
2. Diffusion vectors in MRSU scheme are simply solution vectors with supremum eigenvalue as a coefficient. This makes the scheme robust. Moreover, no complicated Jacobian matrices are involved in the diffusion terms.
3. It is easy to extend MRSU scheme from scalar to vector conservation laws.

The efficacy of the proposed scheme is shown by solving various one and two dimensional test cases for Burgers equation (which includes both convex and non-convex flux function), Euler equations and shallow water equations.

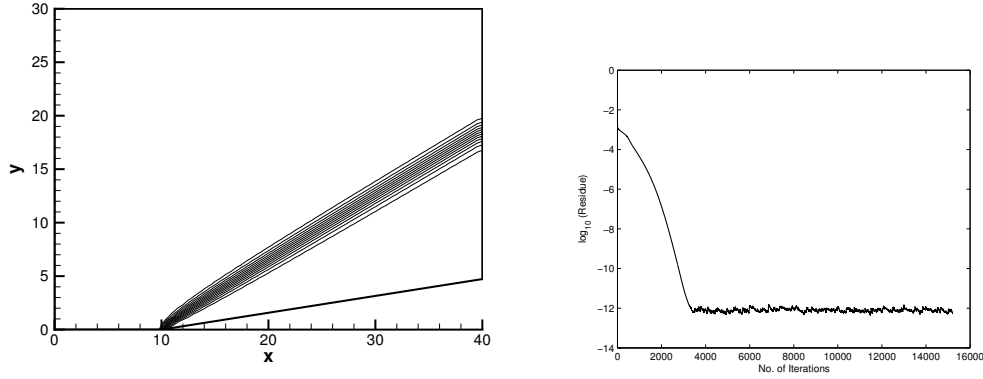


Figure 31: Hydraulic jump using  $80 \times 60$  Q4 mesh and Residue plots.

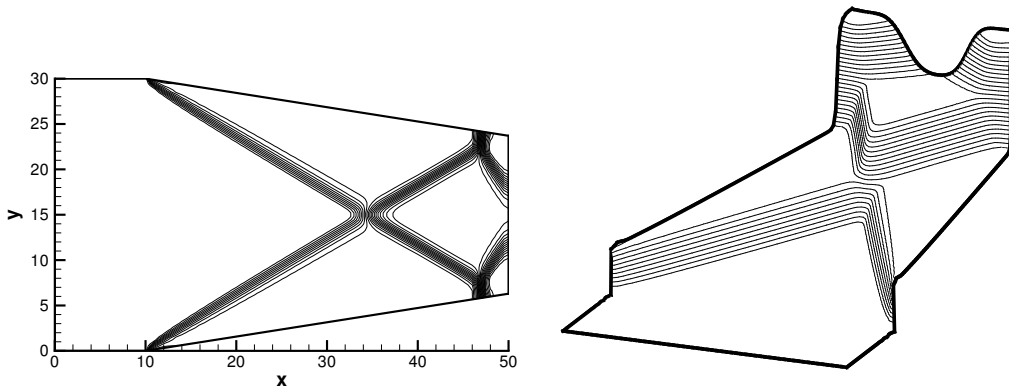


Figure 32: Hydraulic jump interaction problem using  $100 \times 60$  contour plots (left) and surface plot (right).

For Euler equations the variations in Mach number is from 0.5 to 20 which covers subsonic, transonic and supersonic regime. This shows the capability of proposed scheme of handling wide range of problems. Moreover, spectral stability analysis is done which gives the expression for critical time step and error analysis shows the optimal convergence rate for the proposed scheme. The proposed scheme is easy to implement in the existing code of stabilized finite element schemes without much modification.

### 13. Acknowledgment

I would like to thank Prof. A.S.Vasudeva Murthy, Tata Institute of Fundamental Research - Centre for Applicable Mathematics, Bangalore and Prof. C.S. Jog, Department of Mechanical Engineering, Indian Institute of Science, Bangalore for giving constructive comments and suggestions which helped me to improve the quality of the manuscript.

### 14. Appendix

#### Derivation of F for one dimensional three discrete velocity model

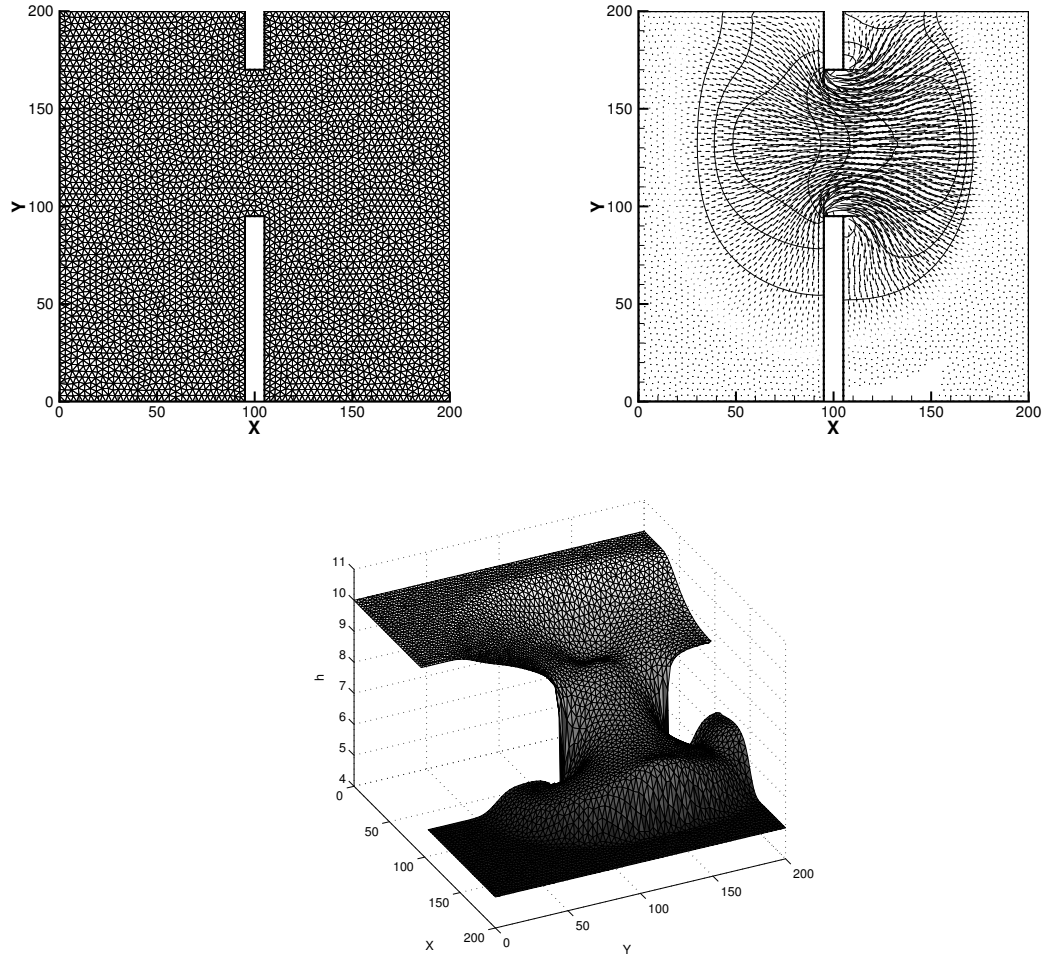


Figure 33: Dam break problem

Let

$$\mathbf{F} = \{F_1 \ F_2 \ F_3\}^T$$

Then, the moments relations are satisfied as

$$\begin{aligned} F_1 + F_2 + F_3 &= U \\ \lambda F_1 + \lambda F_2 + \lambda F_3 &= G(U) \end{aligned} \quad (9)$$

Using three velocity model the  $\Lambda$  matrix is given as

$$\Lambda = \begin{bmatrix} -\lambda & 0 & 0 \\ 0 & 0 & 0 \\ 0 & 0 & \lambda \end{bmatrix}$$

which makes the last moment relation as

$$F_3 - F_1 = \frac{G(U)}{\lambda} \quad (10)$$

Assuming  $\mathbf{F}$  as a linear combination of  $U$  and  $G(U)$  as

$$\mathbf{F} = \begin{Bmatrix} F_1 \\ F_2 \\ F_3 \end{Bmatrix} = \begin{Bmatrix} c_1 U + d_1 G(U) \\ c_2 U + d_2 G(U) \\ c_3 U + d_3 G(U) \end{Bmatrix}$$

Using moment relations (9) and (10) following relations are obtained

$$\begin{aligned} \sum_{i=1}^3 c_i &= 1 \\ \sum_{i=1}^3 d_i &= 0 \\ (c_3 - c_1)U + (d_3 - d_1)G(U) &= \frac{G(U)}{\lambda} \end{aligned}$$

Choosing  $c_1 = c_2 = c_3 = \frac{1}{3}$  and  $d_1 = \frac{-1}{2\lambda} = -d_3$ ,  $d_2 = 0$ . This gives

$$\mathbf{F} = \begin{Bmatrix} \frac{U}{3} - \frac{G}{2\lambda} \\ \frac{U}{3} \\ \frac{U}{3} + \frac{G}{2\lambda} \end{Bmatrix}$$

## References

- [1] O.C.Zienkiewicz, R.L.Taylor, The Finite Element Method, Volume 3, 6<sup>th</sup> edition, Butterworth-Heinemann, 2005.
- [2] Bochev P.B., Gunzburger M.D., Least-Squares Finite Element Methods. Springer, 2009.
- [3] Hesthaven J.S., Warburton T., Nodal Discontinuous Galerkin Methods. Springer, 2008.
- [4] Donea J., Huerta A. : Finite element methods for flow problems, Wiley, 2003.
- [5] Chung T.J., Finite element analysis in fluid dynamics.McGraw-Hill international, 1978.
- [6] Tezduyar TE, Huges TJR, .Finite element formulation of convected dominated flows with particular emphasis on the compressible Euler equations. In: Proceedings of AIAA 21st aerospace sciences meeting. AIAA Paper 83-0125, Reno, Nevada (1982).
- [7] Tezduyar TE, Senga M. SUPG finite element computation of inviscid supersonic flows with  $YZ\beta$  shock-capturing. *Computers and Fluids*, 36: 147-159, 2007.
- [8] Jagtap, Ameya D., Kinetic Streamlined Upwind Petrov-Galerkin methods for hyperbolic partial differential equations, PhD thesis, Indian Institute of Science, Bangalore,India, July 2015.
- [9] Jin S., Xin Z., The relaxation schemes for system of conservation laws in arbitrary space dimensions, *Communications in pure and applied Mathematics*, vol. 48, no. 3, 235-277, 1995.
- [10] A. S. Vasudeva Murthy, An alternative relaxation approximation to conservation laws, *Journal of Computational and Applied Mathematics*, 203 (2007) 437-443
- [11] Schroll H., High resolution relaxed upwind schemes in gas dynamics, *J. Sci. Comput.* 17 (2002), pp. 599-607.
- [12] Li, X., Yu X. and Chen G., The third order relaxation schemes for hyperbolic conservation laws, *J. Comp. Appl. Math.*, 138 (2002), pp. 93-108.
- [13] Seaid M., Improved applications of relaxation schemes for hyperbolic systems of conservation laws and convection-diffusion problems, *Computational methods in applied mathematics*, vol.6 (2006), No. 1, pp.56-86.
- [14] Chen G. Q., Levermore C.D. and Liu T.P., Hyperbolic conservation laws with stiff relaxation terms and entropy, *Comm. Pure Appl. Math.* 47 (1994), pp. 787-830.
- [15] Chalabi A., Convergence of relaxation scheme for hyperbolic conservation laws with stiff source terms, *Math. Comput.* 68 (1999), pp. 955-970.
- [16] Fan H., Jin S. and Teng Z., Zero reaction limit for hyperbolic conservation laws with source terms, *J. Diff. Equations* 168 (2000), pp. 270-294.
- [17] Natalini R., A Discrete Kinetic Approximation of Entropy Solutions to Multidimensional Scalar Conservation Laws, *Journal of Differential Equations*, vol. 148, 292-317, 1999.
- [18] R. Natalini, Recent mathematical results on hyperbolic relaxation problems, *Analysis of systems of conservation laws*, Pitman Research Notes in Mathematics Series, Longman, Harlow, 1998.
- [19] Aregba-Driollet D., Natalini R., Discrete Kinetic schemes for Multidimensional systems of conservation laws, *SIAM Journal of Numerical Analysis*, vol. 37, no. 6, 1973-2004, 2000.
- [20] Banda M., Variants of relaxed schemes and two dimensional gas dynamics, *Journal of Computational and Applied Mathematics*, vol.175, no. 1, 41-62, 2005.
- [21] Bochut F., Construction of BGK model with a family of kinetic entropies for a given system of conservation laws. *Journal of Statistical Physics* 1999, 95: 113-170.

- [22] Bereux F. and Sainsaulieu L., A Roe-type Riemann solver for hyperbolic systems with relaxation based on a time dependent wave decomposition, *Numerische Mathematik*, vol. 77, 143-185, 1997.
- [23] Cecchi M.M., Redivo-Zaglia M. and Russo G., Extrapolation methods for hyperbolic systems with relaxation, *Journal of Computational and Applied Mathematics*, vol. 66, no. 1-2, 359-375, 1996.
- [24] Cavalli F., et. al., A family of relaxation schemes nonlinear convection diffusion problems. *Communications in Computational Physics*, vol. 5, no. 2-4, 532-545, 2009.
- [25] Hittenger J.A.F. and Roe P.L., Asymptotic analysis of the Riemann problem for the constant coefficient hyperbolic systems with relaxation, *ZAMM-Journal of Applied Mathematics and Mechanics*, vol. 84, no. 7, 452-471, 2004.
- [26] Banda M.K. et. al., A lattice- Boltzmann relaxation scheme for coupled convection-radiation systems, *Journal of Computational Physics*, 226 (2007) 1408 - 1431.
- [27] Graille B., Approximation of mono-dimensional hyperbolic systems: A lattice Boltzmann scheme as a relaxation method, *Journal of Computational Physics*, 266 (2014) 74 - 88.
- [28] Arvanitis C. et. al., Adaptive finite element relaxation schemes for hyperbolic conservation laws, *Mathematical Modeling and Numerical Analysis, ESAIM:M2AN*, Vol. 35, No. 1, 2001, pp 17-33.
- [29] Laney C.B., *Computational Gasdynamics*, Cambridge University Press, 1998.
- [30] Leveque R.J. and Pelanti M., A class of approximate Riemann solvers and their relation to relaxation schemes, *Journal of Computational Physics*, vol 172, 572-591, 2001.
- [31] H.C. Yee, R.F. Warming and A. Harten, A high-resolution numerical technique for inviscid gas-dynamics problems with weak solutions, *Proceedings in eight international conference on numerical methods in fluid dynamics*, Lecture notes in Physics, Vol. 170, Springer, New York/Berlin, pp. 546-552, 1982.
- [32] S. Spekreijse, Multigrid solution of monotone second order discretizations of hyperbolic conservation laws, *Mathematics of Computation*, vol. 49, No. 179, pp. 135-155, 1987.
- [33] H. Viviani, Numerical solution of two dimensional reference test cases. AGARD AR-211: Test cases for inviscid flow field methods, 1985.
- [34] D. Levy, K.G. Powell and B. Van Leer, Use of a rotated Riemann solver for two dimensional Euler equations, *Journal of Computational Physics*, Vol.106, no. 2, 201-214 (1993).
- [35] F.S. Billig, Shock-wave shapes around spherical and cylindrical-nosed bodies, *Journal of Spacecraft and Rockets*, Vol. 4, No. 6 (1967), pp. 822-823.
- [36] C.W. Shu, S. Osher: Efficient implementation of essentially non-oscillatory shock-capturing schemes, II, *Journal of Computational Physics*, 83, 3278 (1989).
- [37] Alexander Kurganov, et. al., Adaptive Semidiscrete Central-Upwind Schemes for Non-convex Hyperbolic Conservation Laws, *SIAM J. Sci. Comput.*, Vol. 29, No. 6, pp. 2381-2401, 2007.
- [38] Harten, A., High Resolution Schemes for Hyperbolic Conservation Laws. *J. Comput. Phys.*, 49:357-293, 1983.
- [39] Hirsch, C., *Numerical Computation of Internal and External Flows*, vol 2, John Wiley and Sons, Chichester, 1990.
- [40] Godunov, Sergei K., Ph.D. Dissertation: Different Methods for Shock Waves, Moscow State University, 1954.
- [41] C. A. J. Fletcher. The Group Finite Element Formulation. *Computer Methods in Applied Mechanics and Engineering*, 37: 225 - 243, 1983.
- [42] K. Morgan and J. Peraire. Unstructured grid finite element methods for fluid mechanics, 1998.
- [43] D. Kuzmin, M. Moller, and S. Turek. HighResolution FEM-FCT Schemes for Multidimensional Conservation Laws. *Computer Methods in Applied Mechanics and Engineering*, 193:4915 - 4946, May 2004.
- [44] D. Kuzmin and S. Turek. HighResolution FEM-TVD Schemes Based on a Fully Multidimensional Flux Limiter. *Journal of Computational Physics*, 198:131 - 158, 2004.
- [45] Benjamin S. Kirk and Graham F. Carey. Development and Validation of a SUPG Finite Element Scheme for the Compressible Navier-Stokes Equations using a Modified Inviscid Flux Discretization. *International Journal for Numerical Methods in Fluids*, 57(3): 265 - 293, 2008.
- [46] Deconinck, H., Paillere, H., Struijs, R., and Roe, P. (1993). Multidimensional upwind schemes based on fluctuation-splitting for systems of conservation laws. *Computational Mechanics*, 11:323 - 340.
- [47] Brooks AN, Hughes TJR (1982) Streamline upwind/Petrov-Galerkin formulations for convection dominated flows with particular emphasis on the incompressible Navier's-Stokes equations. *Comput Methods Appl Mech Eng* 32:199 - 259.
- [48] Hughes TJR, Brooks AN (1979) A multi-dimensional upwind scheme with no crosswind diffusion. In: Hughes TJR (ed) finite element methods for convection dominated flows, AMD-vol 34. ASME, New York, pp 19 - 35
- [49] Catabriga L., Coutinho A.L.G.A., Improving convergence to steady state of implicit SUPG solution of Euler equations, *Commun. Numer. Meth. Engng* 2002, 18:345 - 353.
- [50] Tezduyar TE (1992) Stabilized finite element formulations for incompressible flow computations. *Adv Appl Mech* 28:1 - 44.
- [51] Tezduyar TE, Hughes TJR (1983) Finite element formulations for convection dominated flows with particular emphasis on the compressible Euler equations. In: Proceedings of AIAA 21st aerospace sciences meeting. AIAA Paper 83-0125, Reno, Nevada.
- [52] Tezduyar TE, Hughes TJR (1982) Development of time-accurate finite element techniques for first-order hyperbolic systems with particular emphasis on the compressible Euler equations. NASA Technical Report NASA-CR-204772, NASA.
- [53] Hughes TJR, Tezduyar TE (1984) Finite element methods for first-order hyperbolic systems with particular emphasis on the compressible Euler equations. *Comput Methods Appl Mech Eng* 45:217 - 284.
- [54] Hughes TJR, Franca LP, Mallet M (1987) A new finite element formulation for computational fluid dynamics: VI. Convergence analysis of the generalized SUPG formulation for linear time-dependent multi-dimensional advective-diffusive systems. *Comput Methods Appl Mech Eng* 63:97 - 112.
- [55] Le Beau GJ, Tezduyar TE (1991) Finite element computation of compressible flows with the SUPG formulation. In: Advances in finite element analysis in fluid dynamics, FED-vol. 123. ASME, New York, pp 21 - 27.
- [56] Lattanzio C. and Serre D., Convergence of a relaxation scheme for hyperbolic systems of conservation laws, *Numer. Math.*, **88**(2001) 121 - 134.
- [57] F. Alcrudo and P. Garcia-Navarro, A high resolution Godunov type scheme in finite volumes for 2D shallow-water equations, *International*

- Journal for Numerical Methods in Fluids 16(6), 489 - 505 (1993).
- [58] Natalini R., Convergence to equilibrium for relaxation approximations of conservation laws, *Comm. Pure Appl. Math.*, **49** (1996) 795 - 823.
  - [59] Toro, E.F., *Riemann Solvers and Numerical Methods for Fluid Dynamics: A practical Introduction*, Springer -Verlag, 3rd edition, 2009,
  - [60] Liska, R. and Wendroff, B., Comparison of several difference schemes in 1D and 2D Test Problems for Euler Equations. *SIAM Journal of Scientific Computation*, 25:995 - 1017, 2003.
  - [61] Xu, W.Q., Relaxation limite for piecewise smooth solutions to conservation laws, *J. Diff. Eq.* **162** (2000), 140 - 173.
  - [62] Zhang, S.Q., Ghidaoui, M.S., Gray, W.G., Li,N.Z., A kinetic flux vector splitting scheme for shallow water flows, *Advances in Water Resources* 26 (2003) 635 - 647.
  - [63] Zoppou, C., Roberts, S., Explicit schemes for dam-break simulations, *J. Hydraul. Eng.* 129 (1), 11 - 34 (2003).
  - [64] Woodward P., Colella P., The numerical solution of two dimensional fluid flow with strong shocks, *Journal of Compu. Phys.*, vol. 54, No.1, 115 - 173, 1984.